

University of Mississippi

eGrove

Honors Theses

Honors College (Sally McDonnell Barksdale
Honors College)

Spring 5-8-2022

A Study of Cannabigerolic Acid and its Derivatives via Raman Spectroscopy and Density Functional Theory

Trevor Wolfe

Follow this and additional works at: https://egrove.olemiss.edu/hon_thesis

 Part of the [Computational Chemistry Commons](#), and the [Physical Chemistry Commons](#)

Recommended Citation

Wolfe, Trevor, "A Study of Cannabigerolic Acid and its Derivatives via Raman Spectroscopy and Density Functional Theory" (2022). *Honors Theses*. 2535.

https://egrove.olemiss.edu/hon_thesis/2535

This Undergraduate Thesis is brought to you for free and open access by the Honors College (Sally McDonnell Barksdale Honors College) at eGrove. It has been accepted for inclusion in Honors Theses by an authorized administrator of eGrove. For more information, please contact egrove@olemiss.edu.

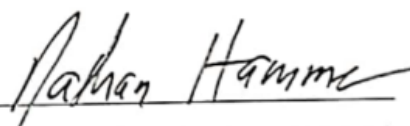
A STUDY OF CANNABIGEROLIC ACID AND ITS DERIVATIVES VIA RAMAN
SPECTROSCOPY AND DENSITY FUNCTIONAL THEORY


By
Trevor J. Wolfe


A thesis submitted to the faculty of the University of Mississippi in partial
fulfillment of the requirements of the Sally McDonnell Barksdale Honors College

Oxford, MS
May 2022

Approved by:


Dr. Nathan I. Hammer (Advisor)


Dr. Ryan C. Fortenberry (Reader)


Dr. Hoang V. Le (Reader)

Copyright © 2022
Trevor J. Wolfe
ALL RIGHTS RESERVED

ACKNOWLEDGEMENTS

First and foremost I would like to thank Dr. ElSohly, Dr. Radwan, and the Marijuana Project for granting me the opportunity to study the samples featured in this work. Without their cooperation, none of this would have been possible. I would also like to acknowledge that the Marijuana Project is funded by the National Institute on Drugs of Abuse (NIDA). I also thank my parents for granting me the opportunity to continue on in my educational career. If it was not for their continued financial and emotional support, I would not have gotten this far. As I continue on to grad school and beyond, I only hope I can keep making you proud. To Dr. Hammer and the rest of the Hammer lab, thank you so much for welcoming me to the group and giving me the opportunity to conduct my research. I will surely miss each and every one of you when I leave for the University of Wisconsin, and I hope whatever lab I join in the future has the same sense of comradery. Special shout out to Ethan Lambert and Cameron Smith, whose combined knowledge helped me understand how to use the Raman spectrometer and thus conduct my research. Although not a member of our group, I am also grateful for Seth Darlington and his random shenanigans in lab, as they made even the dullest of days more enjoyable. Last but not least, I want to thank Nick Kruse for being a great friend by supporting me even when I doubted myself. I know you will go on to accomplish great things in life, and even though I'll be all the way in Wisconsin I hope I'll still be able to reciprocate the support you've given me.

ABSTRACT

The cannabinoids are a class of molecules endogenous to the cannabis plant. Their scientific relevance has increased in recent years due to the mercurial legal status of marijuana across the United States. Some of the most known are cannabidiol (CBD), δ^9 -tetrahydrocannabinol (δ^9 -THC), and δ^8 -THC due in large part to their widespread use, especially in states where marijuana and related products are legal. However, cannabigerolic acid (CBGA) is arguably the most important cannabinoid; it is enzymatically converted into other acidic cannabinoids, which subsequently undergo non-enzymatic processes (isomerization, thermal decarboxylation, oxidation, etc.) to synthesize further cannabinoids. Although there is a wealth of research regarding these compounds, there are not any examples in the literature of the analysis of the vibrational spectroscopic differences between them as they undergo the different conversion processes. Thus, the goal of this current research was to utilize Raman spectroscopy to collect high resolution spectra for each available cannabinoid in order to highlight key vibrational spectroscopic differences between them. These vibrational differences were subsequently analyzed in the context of the biosynthetic pathways stemming from CBGA. Density functional theory (DFT) calculations were also utilized to generate simulated spectra in order to evaluate the extent of agreement between experiment and theory. The results of this study demonstrate that key vibrational differences, particularly in the OH stretching region, could be identified between the spectra. Additionally, the overall agreement between experiment and theory was good, although it varied depending on the sample.

TABLE OF CONTENTS

ACKNOWLEDGEMENTS.....	3
ABSTRACT.....	4
LIST OF FIGURES.....	7
CHAPTER I: INTRODUCTION TO THE CANNABINOIDS.....	9
1.1 BIOSYNTHESIS.....	9
1.2 RELEVANCE OF STUDY.....	12
CHAPTER II: RAMAN SPECTROSCOPY.....	14
2.1 OVERVIEW OF SPECTROSCOPY AND SCATTERING.....	14
2.2 VIBRATIONAL ENERGY LEVELS.....	15
2.3 POLARIZABILITY.....	18
2.4 BASIC INSTRUMENTATION.....	19
CHAPTER III: COMPUTATIONAL CHEMISTRY.....	22
3.1 OVERVIEW OF THE SCHRÖDINGER EQUATION.....	22
3.2 INTRODUCTION TO COMPUTATIONAL METHODS.....	23
CHAPTER IV: METHODS.....	26
4.1 EXPERIMENTAL SETUP.....	26
4.2 COMPUTATIONAL METHODS.....	27
CHAPTER V: RESULTS.....	28
CHAPTER VI: DISCUSSION OF RESULTS.....	45
6.1 THE CBG PATHWAY.....	45
6.1.1 CBGA.....	45

6.1.2 CBG.....	47
6.2 THE CBD PATHWAY.....	49
6.2.1 CBDA.....	49
6.2.2 CBD.....	53
6.2.3 CBDVA.....	57
6.2.4 CBDV.....	59
6.3 THE THC PATHWAY.....	63
6.3.1 δ^9 -THCA.....	63
6.3.2 δ^9 -THC.....	66
6.3.3 δ^8 -THC.....	68
6.3.4 CBN.....	71
6.4 THE CBC PATHWAY.....	75
6.4.1 CBCA.....	75
6.4.2 CBC.....	77
CHAPTER VII: CONCLUSIONS AND FUTURE WORK.....	81
CHAPTER VIII: REFERENCES.....	83

LIST OF FIGURES

Figure 1.1 Overview of the biosynthesis of cannabinoids starting from CBGA.....	11
Figure 2.1 Energy diagrams depicting the differences between Stokes, Rayleigh, and anti-Stokes scattering.....	15
Figure 2.2 Generalized representation of the energy levels of the Harmonic Oscillator and Morse Potential.....	16
Figure 2.3 The electromagnetic spectrum with emphasis on the visible spectrum.....	20
Figure 5.1 Simulated Raman spectrum of CBGA.....	28
Figure 5.2 Simulated Raman spectrum of CBG.....	29
Figure 5.3 Simulated Raman spectrum of CBDA.....	29
Figure 5.4 Simulated Raman spectrum of CBD.....	30
Figure 5.5 Simulated Raman spectrum of CBDVA.....	30
Figure 5.6 Simulated Raman spectrum of CBDV.....	31
Figure 5.7 Simulated Raman spectrum of δ^9 -THCA.....	31
Figure 5.8 Simulated Raman spectrum of δ^9 -THC.....	32
Figure 5.9 Simulated Raman spectrum of δ^8 -THC.....	32
Figure 5.10 Simulated Raman spectrum of CBN.....	33
Figure 5.11 Simulated Raman spectrum of CBCA.....	33
Figure 5.12 Simulated Raman spectrum of CBC.....	34
Figure 5.13 Experimental Raman spectrum of CBGA.....	34
Figure 5.14 Experimental Raman spectrum of CBG.....	35

Figure 5.15 Experimental Raman spectrum of CBDA.....	35
Figure 5.16 Experimental Raman spectrum of CBD.....	36
Figure 5.17 Experimental Raman spectrum of CBDV.....	36
Figure 5.18 Experimental Raman spectrum of δ^9 -THCA.....	37
Figure 5.19 Experimental Raman spectrum of δ^9 -THC.....	37
Figure 5.20 Experimental Raman spectrum of δ^8 -THC.....	38
Figure 5.21 Experimental Raman spectrum of CBN.....	38
Figure 5.22 Experimental Raman spectrum of CBC.....	39
Figure 5.23 Combined Raman spectra of CBGA.....	39
Figure 5.24 Combined Raman spectra of CBG.....	40
Figure 5.25 Combined Raman spectra of CBDA.....	40
Figure 5.26 Combined Raman spectra of CBD.....	41
Figure 5.27 Combined Raman spectra of CBDV.....	41
Figure 5.28 Combined Raman spectra of δ^9 -THCA.....	42
Figure 5.29 Combined Raman spectra of δ^9 -THC.....	42
Figure 5.30 Combined Raman spectra of δ^8 -THC.....	43
Figure 5.31 Combined Raman spectra of CBN.....	43
Figure 5.32 Combined Raman spectra of CBC.....	44

CHAPTER I: INTRODUCTION TO THE CANNABINOIDS

1.1 – BIOSYNTHESIS

Although there are over 500 identified compounds present in cannabis, only a fraction of them are cannabinoids, which are characterized by terpenic and phenolic substituents and produce psychoactive effects when interacting with the human cannabinoid receptors (CB1 and CB2)^{1,2}. Of these, the following were available for the purposes of this work: CBGA, cannabigerol (CBG), cannabidiolic acid (CBDA), CBD, δ^9 -tetrahydrocannabinolic acid (δ^9 -THCA), δ^9 -THC, δ^8 -THC, cannabinol (CBN), cannabichromene (CBC), and cannabidivarin (CBDV). Much research has been conducted in order to understand how the cannabinoids are biosynthesized within the cannabis plant. In the currently accepted conversion scheme, first proposed by Fellermeier et al. in 1998, CBGA is the central precursor from which the other cannabinoids are derived via different synthetic pathways³. Figure 1 provides a clearer illustration of these pathways, and is based on information presented by Degenhardt et al⁴. Of note, this figure only encompasses the biosynthesis of the cannabinoids included in this study, and is by no means a comprehensive overview of every possible synthetic pathway. Furthermore, even though CBDVA and CBCA were not available for study in this current work they are included in the figure because they are precursors to cannabinoids that were studied.

Regarding the biosynthetic pathways of the cannabinoids included in this study, enzymatic conversion, thermal decarboxylation, isomerization, and

oxidation are the major processes. Beginning with enzymatic conversion, there are only three enzymes that interact with CBGA to produce other cannabinoids with carboxylic acid moieties: tetrahydrocannabinolic acid synthase (THCAS), cannabidiolic acid synthase (CBDAS), and cannabichromenic acid synthase (CBCAS)⁴. As can be seen from Figure 1, CBGA is converted into THCA by THCAS, CBDA and CBDVA by CBDAS, and CBCA by CBCAS. A common feature of all three enzymes is that their products have an increased number of cyclic rings compared to CBGA. For instance, THCAS interaction with CBGA causes a bond to form between the *para*-OH group (in relation to the carboxylic acid moiety) and the final branched carbon of the terpene tail, thereby forming a cyclic ring between the phenol and the newly formed monoterpene ring⁴. CBDAS, on the other hand, only forms the monoterpene ring, thus leaving the *para*-OH of the phenol ring unaffected. Furthermore, CBCAS essentially does the opposite, as it forms a pyran ring through the *para*-OH without cyclizing the terpene tail.

The second major process outlined in Figure 1 is nonenzymatic decarboxylation. In other words, the carboxylic acid group is removed as a result of storage, heat (i.e. from burning and smoking cannabis), or exposure to sunlight⁴. Hence, CBGA is converted into CBG, δ^9 -THCA is converted into δ^9 -THC, CBDA is converted into CBD, and so on. These decarboxylated products can then undergo further natural processes to synthesize additional cannabinoids. For instance, δ^9 -THC is naturally converted into the δ^8 -THC isomer, which effectively moves the position of the double bond in the monoterpene ring (see Figure 1). Furthermore,

δ^8 -THC can be oxidized to CBN, resulting in the removal of four hydrogens from the monoterpene ring and an increase in aromaticity of that region of the molecule.

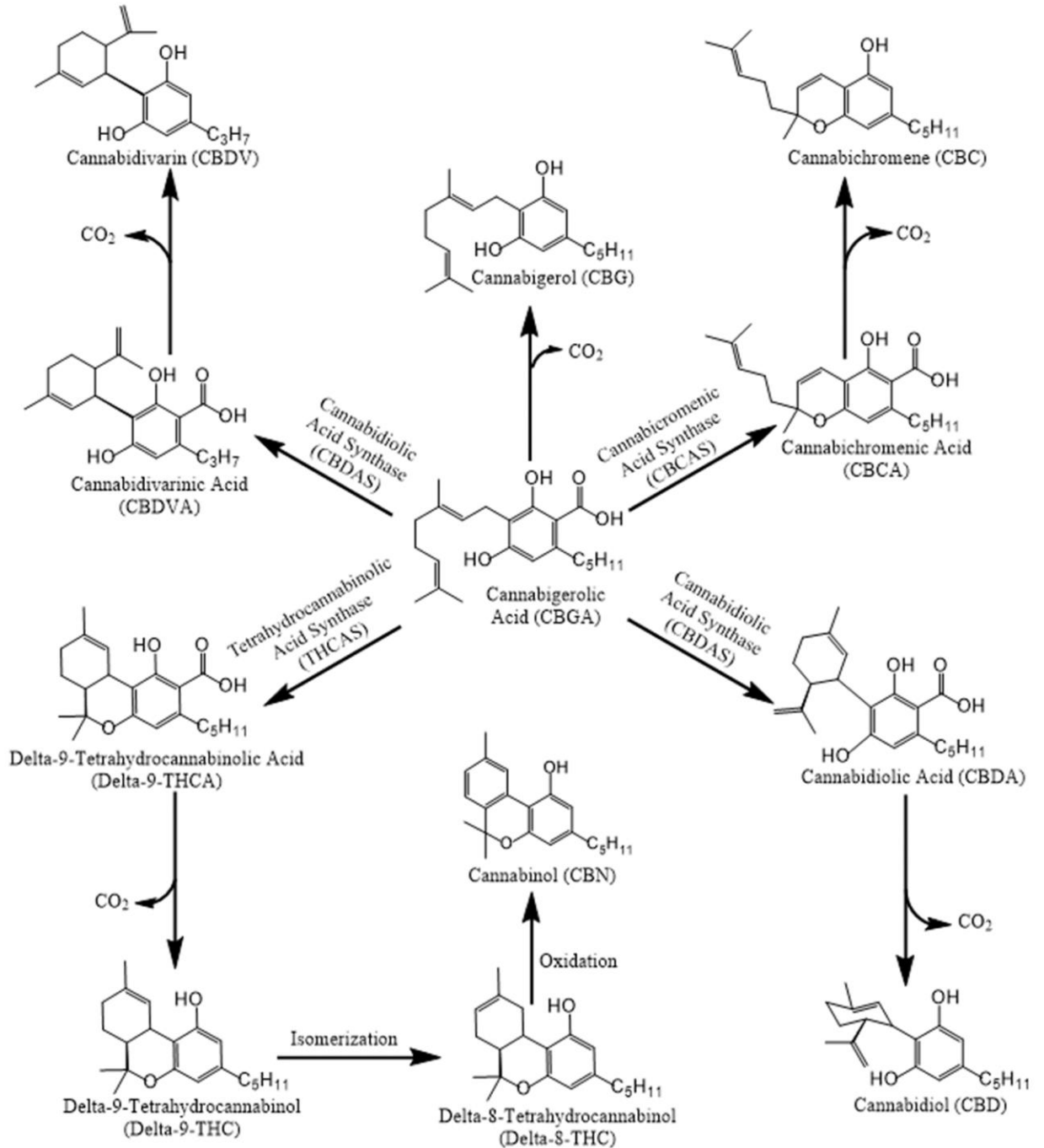


Figure 1.1: Overview of the biosynthesis of cannabinoids starting from CBGA.

As can be expected, the structural differences between the cannabinoids impart different properties to each compound. For example, CBG does not produce the same psychotropic effects as δ^9 -THC, however it demonstrates antibacterial properties against gram positive bacteria². Additionally, although the only structural difference between δ^8 - and δ^9 -THC is the location of the double bond in the monoterpene ring, δ^8 -THC is less psychoactive than δ^9 -THC, thus giving rise to an ambiguous legal status in which certain states have restricted or banned its sale while others have not^{5,6}. Moreover, CBD does not have the same psychoactivity as δ^9 -THC, however it has anti-inflammatory, antioxidant, and anticonvulsant properties, the latter of which has led to the prescription of CBD for treatment of neurological conditions such as epilepsy⁷⁻⁹. Not only do the effects on the body differ between the cannabinoids, their physical properties differ as well. One such property, molecular vibration, can be probed using various spectroscopic techniques including Raman spectroscopy. This will be discussed in greater detail in the following chapter.

1.2 – RELEVANCE OF STUDY

Despite marijuana remaining illegal on the federal level, a growing number of states have legalized its use either medicinally or recreationally. As more states follow suit, the access to marijuana, and thus the cannabinoids present within, will increase. Numerous studies investigating the prevalence of cannabis use within various populations have been conducted in recent years. For example, one study from 2017 found that 6% and 24% of middle and high school students, respectively,

reported ever smoking a blunt¹⁰, which is a method of using cannabis in which the dried plant is rolled and smoked like a cigarette. Additionally, a national survey from 2001 found that 5% of youth aged 12-17 years reported blunt use in the past 30 days¹¹. Generally speaking, cannabis use is more prevalent in adults aged 18-34 years, as a national study of this age range indicated that 21% reported use of cannabis in the past 12 months¹². Further data regarding cannabis use across other populations and various methods of usage can be found in a systematic review by Wadsworth et al¹³. Considering that these statistics may increase as marijuana is legalized across more states, research focusing on the properties of cannabinoids is especially relevant.

From a forensic point of view, there are examples in the literature of Raman spectroscopy being used to identify common drugs of abuse, including cannabinoids¹⁴. In essence, if someone is arrested for the possession of a substance suspected to contain δ^9 -THC, crime labs equipped with Raman spectrometers can use this technique to confirm its presence in the sample. Since one of the goals of this project was to collect the highest resolution Raman spectra possible for each cannabinoid studied, the results provided herein could be added to existing spectral libraries used by law enforcement for drug analysis. In other words, the experimental spectra could be used as a point of comparison between the isolated and purified cannabinoids and what is present in a piece of questioned drug evidence.

CHAPTER II: RAMAN SPECTROSCOPY

2.1 – OVERVIEW OF SPECTROSCOPY AND SCATTERING

Before introducing the principles of Raman spectroscopy, it is important to first define what spectroscopy itself is. Simply put, spectroscopy is the study of the interaction between matter and electromagnetic radiation¹⁵. Spectroscopic techniques are typically based on one of the following phenomena: emission, absorption, fluorescence, or scattering¹⁶. Raman spectroscopy belongs to the latter category. More specifically, it is based on the Raman Effect, which states that a small fraction of scattered light has a different frequency, and thus different energy, than the incident monochromatic light¹⁵. This type of scattering is therefore inelastic, and can be further subdivided into two forms: Stokes and anti-Stokes. Stokes scattered light has less energy than the incident light, whereas anti-Stokes scattered light has greater energy¹⁷. Figure 2 provides a better illustration of the differences between each form of scattering. To briefly explain, when photons from the incident light source interact with a molecule, the molecule is promoted to a short lived virtual state, after which it relaxes to a vibrational state of the same energy (Rayleigh), higher energy (Stokes), or lower energy (Rayleigh) than the starting vibrational state¹⁷. Because Stokes scattering involves a transition to a higher energy vibrational state, Stokes shifted Raman bands are more intense than anti-Stokes bands¹⁵. Of note, the probability of Stokes scattering is roughly one in a million, while the probability for anti-Stokes is even lower.

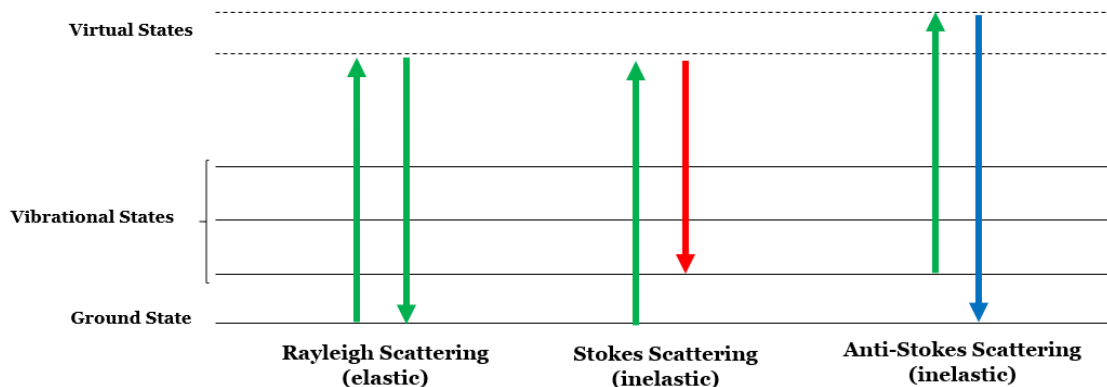


Figure 2.1: Energy diagrams depicting the differences between Stokes, Rayleigh, and anti-Stokes scattering.

2.2 – VIBRATIONAL ENERGY LEVELS

Another important consideration when discussing a spectroscopic method is the energy level it is able to analyze. Most spectroscopic methods are able to probe four different energy levels: translational, rotational, vibrational, and electronic. Of these, translational is the lowest in energy, while electronic is the highest. Since Raman spectroscopy is a vibrational technique, the other energy levels will not be discussed in greater detail. Vibrational energy levels stem from the intrinsic stretching and bending that occurs between bonded atoms. A simpler way to visualize a molecule's vibrational energy levels is to use the Harmonic Oscillator model. In this idealized model, atoms are depicted as being connected by a rigid spring that represents the bond between them¹⁸. The linear restoring force acting on a harmonic oscillator can be mathematically determined through Hooke's Law, which is written as follows¹⁸:

$$F = -kx \quad \text{(Equation 2.1)}$$

In the above equation, F is the force acting on the spring to return it to its original state, k is the rigidity of the spring, and x is the displacement of the string. The graph of the energy levels of an idealized harmonic oscillator is represented by the blue parabola in Figure 2.2, with bond length on the x-axis and energy on the y-axis. The lowest point of the parabola represents the bond length at which the vibrational mode is at its lowest energy. As the bond length gets smaller, the distance between the nuclei of the bonded atoms also gets smaller, thus intensifying internuclear repulsion forces and increasing the energy of the bond. On the other hand, as the bond length increases beyond the minimum energy value, there is a greater tendency for the two atoms to dissociate. As a result, the bond energy increases until it is no longer energetically favorable for the atoms to remain bonded, at which point the bond is broken. The energy required to break an atomic bond is termed the bond dissociation energy, and is represented by the horizontal dashed line in Figure 2.2.

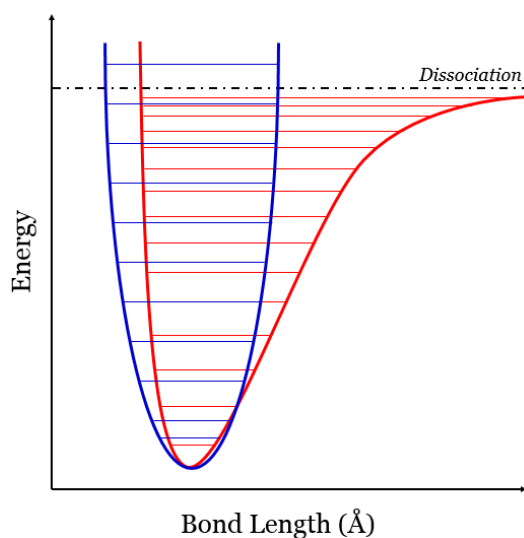


Figure 2.2: Generalized representation of the energy levels of the Harmonic Oscillator and Morse Potential.

An important feature of the Harmonic Oscillator model is that vibrational energy levels, represented by the lines in the parabola, are predicted to be evenly spaced as the energy increases. In other words, the energy required to transition from the first to second vibronic state is the same as is required to transition from the fourth to fifth. The other major aspect of the Harmonic Oscillator is the regular parabolic shape of the graph. In other words, the rate of energy change is constant whether the atomic radius decreases or increases. It is important to note that, in reality, the prior two characteristics are not observed experimentally. Rather, the Morse Potential is a more accurate representation of the effects of atomic radius on bond energy, and is depicted by the red graph in Figure 2.2. Of note, rather than being evenly spaced, the vibrational energy levels get closer together as the bond energy increases. In essence, the energy gap between vibrational levels gets smaller, thus making transitions between higher level vibrational levels easier. Another key difference between the Morse Potential and Harmonic Oscillator is that the graph plateaus near the bond dissociation energy as the bond length increases, meaning the rate energy change decreases.

It is also important to discuss some of the theory behind molecular vibrations in order to effectively describe Raman spectroscopy. For one, each peak in a Raman spectrum correlates to a vibrational mode in the molecule, which in turn represents a transition from one vibrational energy level to another. For linear molecules, the number of expected vibrational modes can be determined by

$$3N-5 \qquad \qquad \qquad \textbf{(Equation 2.2)}$$

whereas for nonlinear molecules it is

$$3N-6$$

(Equation 2.3)

In the above equations, N represents the total number of atoms in the molecule. The coefficient of 3 comes from the fact that, in the standard three coordinate Cartesian system, each atom has 3 degrees of freedom¹⁹. Since only the vibrational modes are being considered, the rotational and translational modes must be subtracted. For a nonlinear molecule, this number is 6, which originates from the fact that there are 3 modes each for translational and rotational motion (one for each axis of translation/rotation). On the other hand, a linear molecule has one less rotational degree of freedom, since a rotation through the axis of the bonded atoms would not change their position. Therefore, only 5 modes are subtracted to yield only the vibrational modes. As an example of this concept, consider a nonlinear molecule with 50 total atoms. Using Equation 2.3, the total predicted vibrational modes would amount to 144. However, the equation does not account for molecular symmetry, so the number of experimentally observed vibrational modes may not always agree with what is predicted.

2.3 – POLARIZABILITY

A final consideration for the theory of Raman spectroscopy is that, in order for a vibrational mode to be Raman active, there must be a net change in polarizability during the vibration. Polarizability is defined as the ease at which the electron cloud of an atom can be distorted, which is generally determined by the extent to which the charge distribution is affected by the nuclear charge²⁰. In general, the more electrons an atom has, the less of an impact the nuclear charge has on the overall charge distribution, therefore resulting in greater

polarizability²⁰. In other words, a larger electron cloud has a higher overall negative charge, which effectively shields each individual electron from the positive nuclear charge to a greater extent than a smaller electron cloud. As a result, a larger electron cloud is less bound to the nucleus and is thus easier to distort. In the context of a molecular vibration, if the bond length between a central and terminal atom increases, then the nuclear charge of the central atom has less of an effect on the electrons of the terminal atom, thus leading to an increase in polarizability. The opposite is true if a terminal atom moves closer to the central atom. To understand how a vibration either does or does not produce a net change in polarizability, consider the linear molecule CO₂. In the case of a symmetric stretch, both oxygen atoms move towards or away from the central carbon atom. Because the polarizability of each oxygen atom changes in the same manner, this particular vibrational mode would be Raman active. However, in the case of the asymmetrical stretch, one oxygen moves towards the carbon while the other moves away. Therefore, the polarizability of one increases while the other decreases, resulting in the net polarizability remaining the same. As a result, this particular mode would be Raman inactive.

2.4 – BASIC INSTRUMENTATION

Moving on from the theories and principles, it is important to also discuss the basic instrumental setup for Raman spectroscopy. Like with other vibrational spectroscopic techniques, one of the most important components is the incident light source. For a Raman spectrometer, the light source is monochromatic, meaning there is only one wavelength, and thus one color, of light present. In the

past, this was commonly achieved through the use of mercury arc lamps. However, as technology improved lasers became the de facto light source¹⁵. Lasers of different wavelengths can be produced by a variety of excitation sources, including argon ion (488 and 514.5 nm), krypton ion (530.9 and 647.1 nm), and helium-neon (He-Ne, 632.8 nm)¹⁵. The excitation source of the laser used in this study was a frequency-doubled neodymium-doped yttrium alumina garnet (Nd:YAG) crystal, which produced a final wavelength of 532 nm. In the visible spectrum of light, this corresponds to a green color. For reference, a diagram of the full electromagnetic spectrum with a zoomed in view of the visible spectrum is included in Figure 2.3.

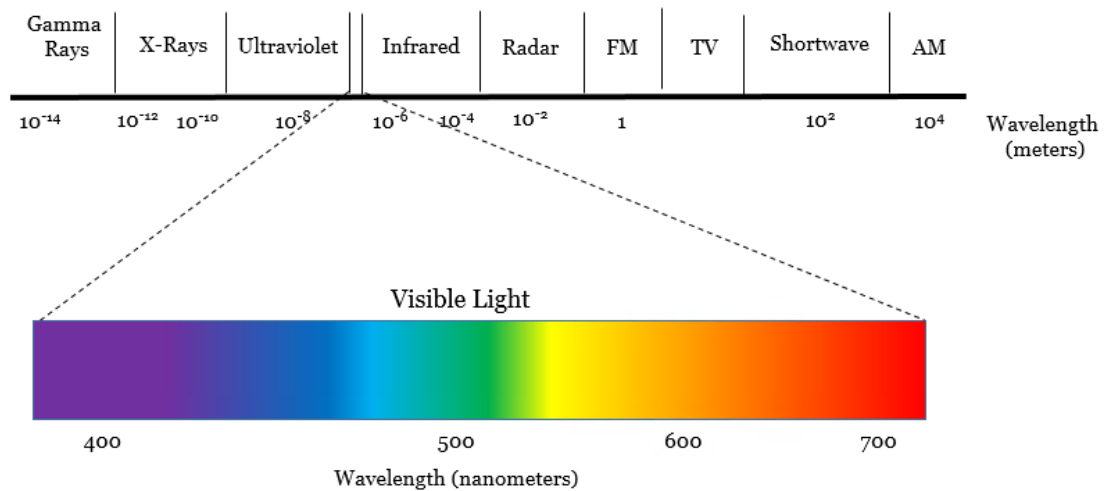


Figure 2.3: The electromagnetic spectrum with emphasis on the visible spectrum.

Once the laser has irradiated the sample, the spectrometer must separate the different wavelengths of scattered light and direct them to the detector so that they may be analyzed and converted into a spectrum. There are a number of ways for the scattered light to be separated. For instance, dispersive Raman

spectrometers use either a prism or a diffraction grating, whereas Fourier-Transform Raman spectrometers employ a Michelson Interferometer¹⁵. While photomultiplier tubes and photodiode arrays were once used as the detectors, they have since been replaced by more sensitive charge transfer devices (CTDs), such as charge-coupled devices (CCDs) and charge-injection devices (CIDs)¹⁵. Regardless of the detector used, its main function is to transform the raw data into a form that can be analyzed and converted into the final Raman spectrum by computer software.

CHAPTER III: COMPUTATIONAL CHEMISTRY

3.1 – OVERVIEW OF THE SCHRÖDINGER EQUATION

Generally speaking, computational chemistry is employed to solve complex chemical and biological problems²¹. For instance, computational methods can be used to optimize molecular geometries, calculate vibrational frequencies, produce simulated Raman spectra, and more²¹. These problems can be approached from a quantum mechanical point of view by determining the wave-like properties of a particle through the Schrödinger Equation, which in its simplified form is written as follows^{22, 23}:

$$\hat{H}\psi = E\psi \quad \text{(Equation 3.1)}$$

In the above equation, \hat{H} represents the Hamiltonian operator, ψ represents the wavefunction, and E represents the total energy of the particle²⁴. Of note, the Hamiltonian itself is the sum of the kinetic and potential energies of the system²⁵. To break it down further, the following terms are accounted for by the Hamiltonian: electron kinetic energy (\hat{T}_e), nuclear kinetic energy (\hat{T}_n), electron-nuclear attraction (\hat{V}_{ne}), electron-electron repulsion (\hat{V}_{ee}), and nuclear-nuclear repulsion (\hat{V}_{nn})^{23, 25-27}.

The Schrödinger Equation can be either time dependent or time independent. The time-independent equation can be solved exactly for a one-electron system (i.e. the hydrogen atom), however the introduction of electron-electron repulsion forces in a multi-electron system prevents the equation from

being solved exactly²⁶. As a result, certain approximations must be used to “solve” the Schrödinger Equation of a multi-electron system. One such approximation is the Born-Oppenheimer approximation, in which nuclear and electron motions are assumed to be separable²³. In essence, due to their much greater mass the nuclei remain fixed in place relative to the electrons²⁵⁻²⁷. This results in the nuclear kinetic energy and nuclear-nuclear repulsion terms of the Hamiltonian changing to zero and a constant value, respectively. Another approximation that can be used is the Hartree-Fock approximation, in which the product of several single-electron systems is used to solve the Schrödinger Equation²³.

3.2 – INTRODUCTION TO COMPUTATIONAL METHODS

There are two main categories of computational methods, which differ in how they approximate the solution of the Schrödinger Equation: *ab initio*, a Latin phrase that translates to “from the beginning,” and semiempirical. As the translation suggests, *ab initio* methods only consider theoretical principles and do not include experimental data²¹. Due to the approximations they employ (i.e. using a simpler functional form of a function or finding the approximate solution to a differential equation), *ab initio* methods provide some of the most accurate approximations to the solution of the Schrödinger Equation²¹. However, the drawback to this increased accuracy is a higher computational cost, which is more severe in larger molecular complexes. For instance, the computational time for the Hartree-Fock method scales by N^4 , where N is the total number of basis functions²¹. Hence, a calculation twice as large actually takes 16 times as long to

complete. Today, the most commonly used *ab initio* method is the Møller and Plesset second order method (MP2)²⁸.

For semiempirical methods, information such as two electron integrals are either approximated or omitted entirely²¹. Naturally, omitting part of a calculation introduces errors, which are subsequently corrected by parameterizing the method²¹. This is achieved by curve-fitting certain parameters or numbers so that there is a high degree of agreement with experimental data²¹. Thus, unlike *ab initio* methods, semiempirical computations rely on experimental data to produce the final result. Due to their simpler nature relative to *ab initio* calculations, a major benefit to semiempirical calculations is their faster computational times²¹. However, a potential drawback is that if the molecule in a calculation differs significantly from the parameterization set, the results could have a considerable degree of inaccuracy²¹. Within the broader category of semiempirical methods lies density functional theory (DFT). DFT takes a one-body quantity approach to the Schrödinger Equation by describing the energy in terms of the overall electron density rather than the many-body wavefunction^{21, 28}. An example of a DFT method is the M06-2X²⁹ functional, which was specifically used for the computational aspects of this current work.

Aside from the method used, a crucial aspect of any theoretical calculation is the basis set. Simply put, a basis set is a set of functions used to define the orbitals^{30, 31}. A wealth of basis sets are available for use, so one must consider the kind of system under study before choosing an appropriate basis set²³. Using

software such as Basis Set Exchange (BSE)³², researchers can choose the atoms present in the molecule of interest and be shown a list of appropriate basis sets.

CHAPTER IV: METHODS

4.1 – EXPERIMENTAL SETUP

The experimental spectra were collected using a LabRAM HR Evolution Raman Spectrometer (Horiba Scientific, Kyoto, Japan) equipped with a charge-coupled device (CCD) camera detector and a 600 grooves/mm diffraction grating. The samples were focused using a 50X LWD objective lens and excited with a 532 nm Nd:YAG laser (Oxxius, Lannion, France) with a spot size of 64 μm . With this instrumental setup, spectral resolution of 1 cm^{-1} could be achieved. Each spectrum was acquired under the following parameters: 50 accumulations, an acquisition time of 2 seconds, and an aperture size of 100 μm . To ensure calibration of the spectrometer, the spectrum of a crystalline Si wafer with a known Raman band at 520 cm^{-1} was recorded prior to analysis of the experimental samples. The spectra were recorded from 200-4000 cm^{-1} , however they are presented here in an abridged form to highlight only the peaks of interest.

The samples used in this study were graciously provided by ElSohly Laboratories. No further sample preparation was done prior to data collection, so the samples were studied as they were given. Specifically, each sample was placed on a glass microscope slide, which was subsequently loaded onto the stage of the spectrometer. Each sample was thus exposed to ambient atmospheric conditions and recorded at room temperature.

4.2 – COMPUTATIONAL METHODS

Geometry optimization and harmonic frequency calculations were performed for each molecule using the Gaussian 16 software suite³³. Due to the large size and relative complexity of the cannabinoids, Density Functional Theory (DFT) calculations were performed using the M06-2X method. The geometry optimizations were performed using three different basis sets of increasing level of theory: 6-31G³⁴, aug-cc-pVDZ³⁵, and aug-cc-pVTZ³⁶. Once the final optimized geometries were produced, the harmonic vibrational frequencies were calculated with the aug-cc-pVTZ basis set. These frequencies were subsequently multiplied by an empirically determined scaling factor of 0.95 to account for anharmonicity and intermolecular interactions. Utilizing the calculated harmonic frequencies and Raman activities, Lorentzian profiles were constructed and summed in order to produce the simulated spectra. As with the experimental spectra, the simulated spectra were abridged to highlight only the peaks of interest.

CHAPTER V: RESULTS

Figures 5.1-5.12 depict the simulated spectra for each cannabinoid, while Figures 5.13-5.22 represent the experimental spectra. As mentioned previously, CBDVA and CBCA were not available for experimental study. However, information can still be garnered from their simulated spectra, so they are included with the caveat that, at this time, they cannot be compared to experimental data. Of note, each spectrum contains the optimized molecular geometry of the respective cannabinoid. For better comparison between experiment and theory, the simulated and experimental spectra are combined into one graph in Figures 5.23-5.32. Also, due to the inherent complexity of the spectra, discussions on the agreement between experiment and theory will focus primarily on select spectroscopic regions. Furthermore, each biosynthetic pathway will be discussed individually, with the spectra of each cannabinoid in the pathway being compared to those of its precursor.

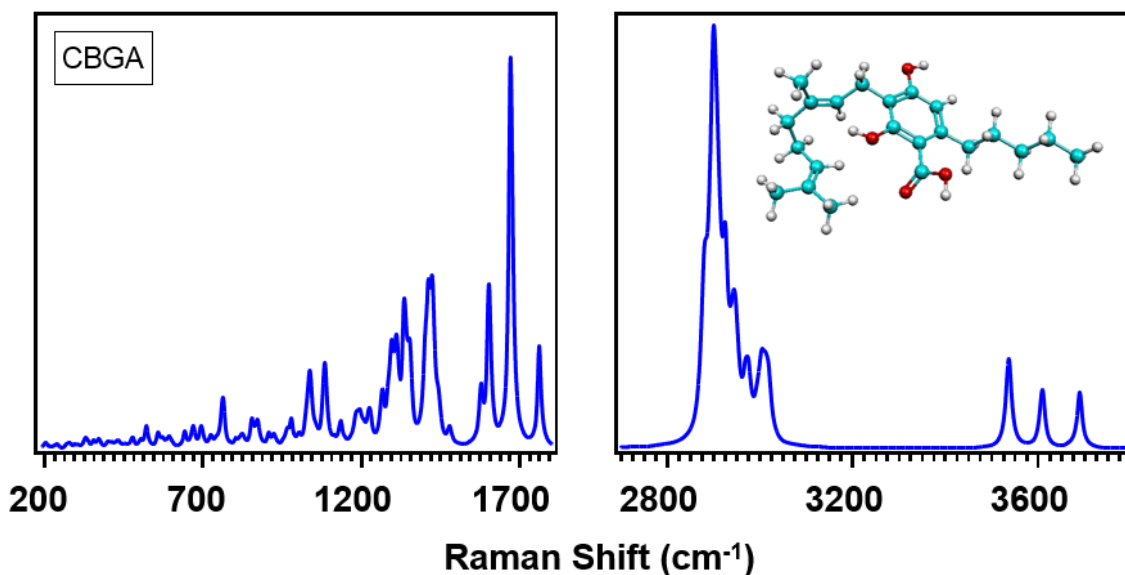


Figure 5.1: Simulated Raman spectrum of CBGA.

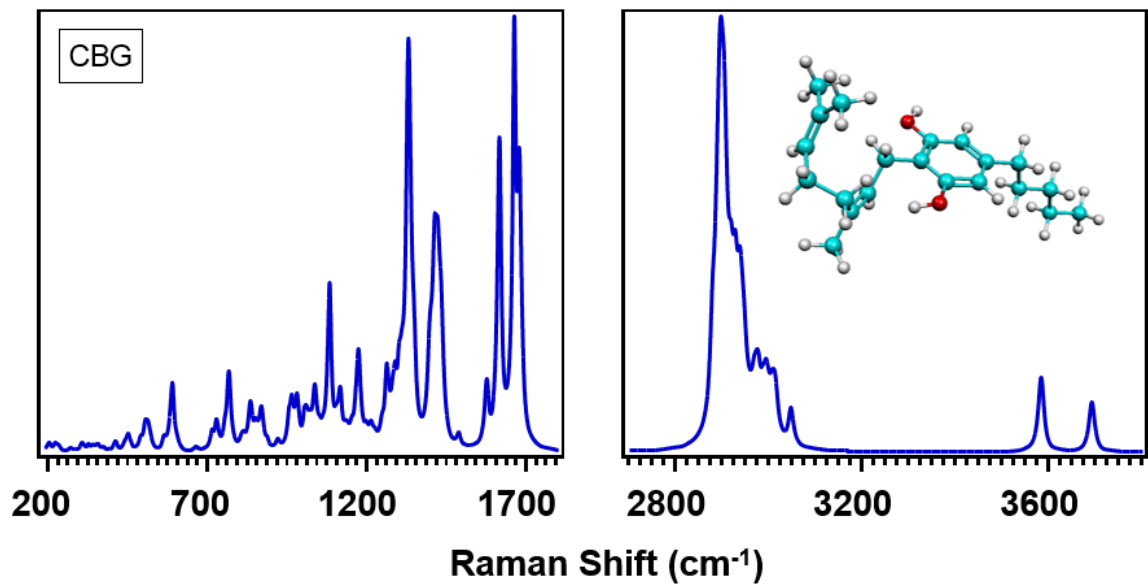


Figure 5.2: Simulated Raman spectrum of CBG.

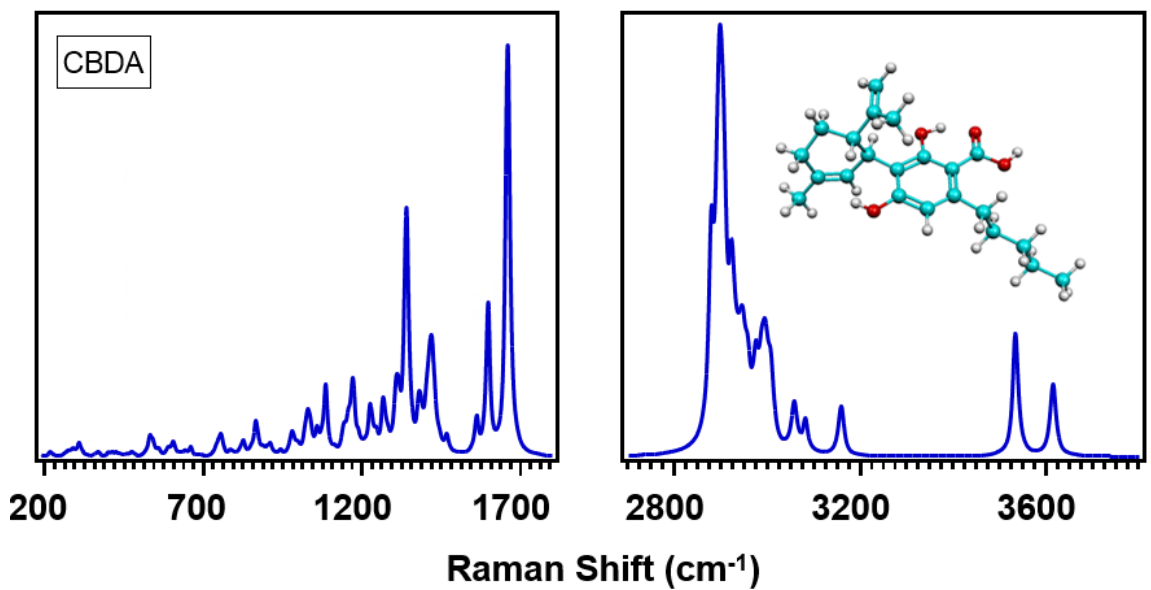


Figure 5.3: Simulated Raman spectrum of CBDA.

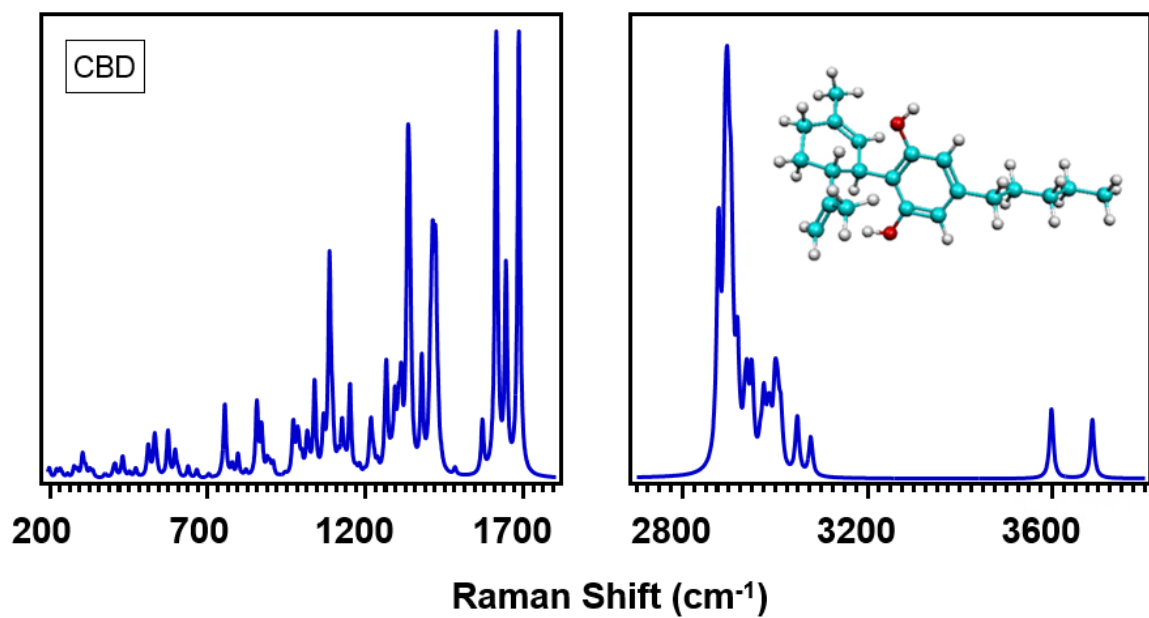


Figure 5.4: Simulated Raman spectrum of CBD.

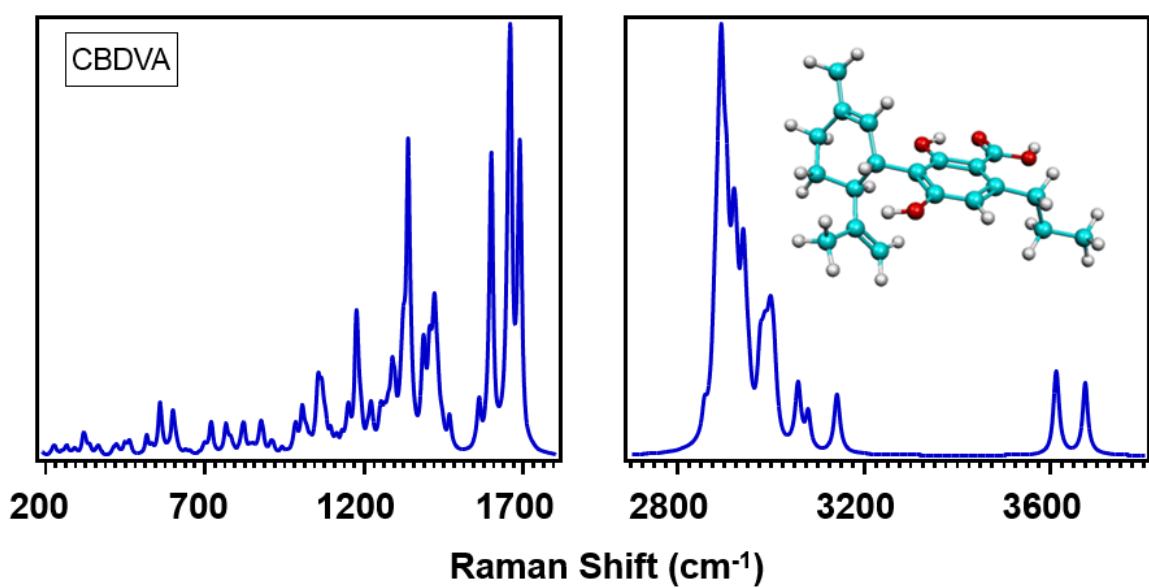


Figure 5.5: Simulated Raman spectrum of CBDVA.

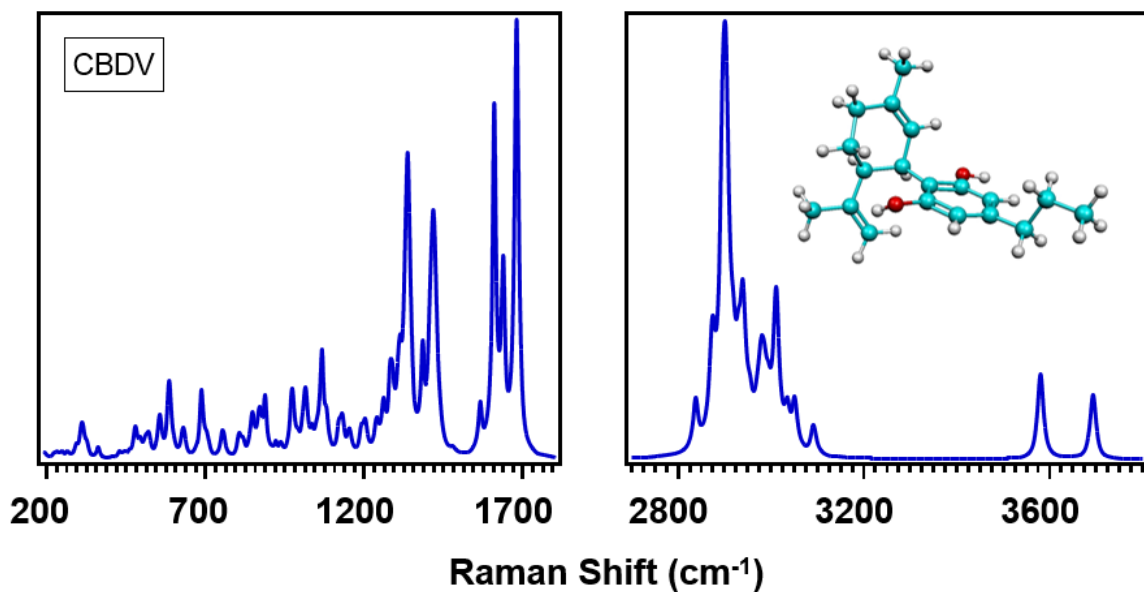


Figure 5.6: Simulated Raman spectrum of CBDV.

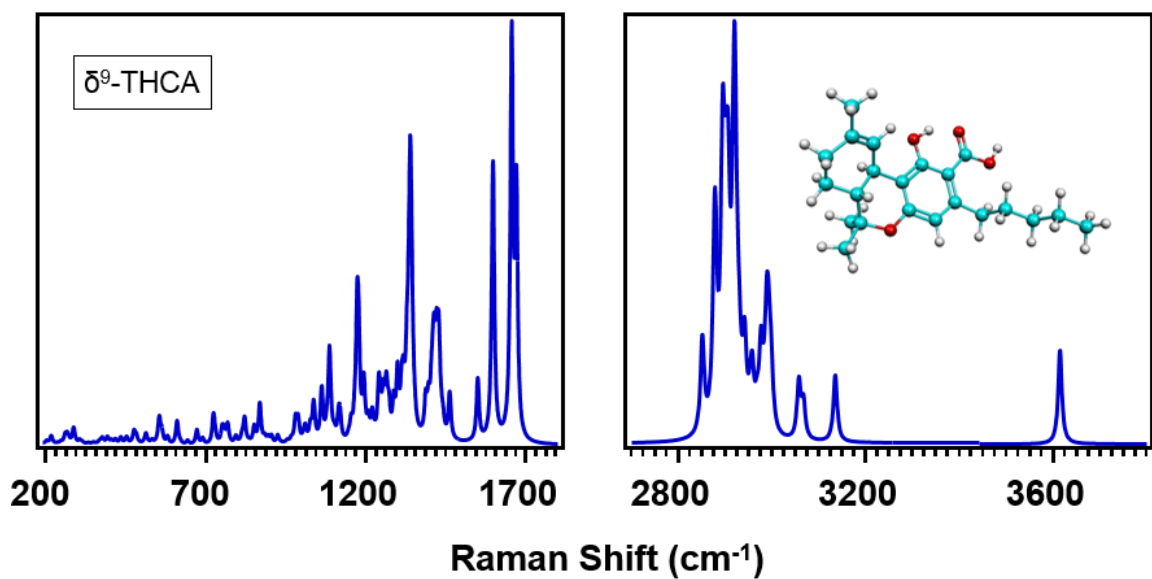


Figure 5.7: Simulated Raman spectrum of δ^9 -THCA.

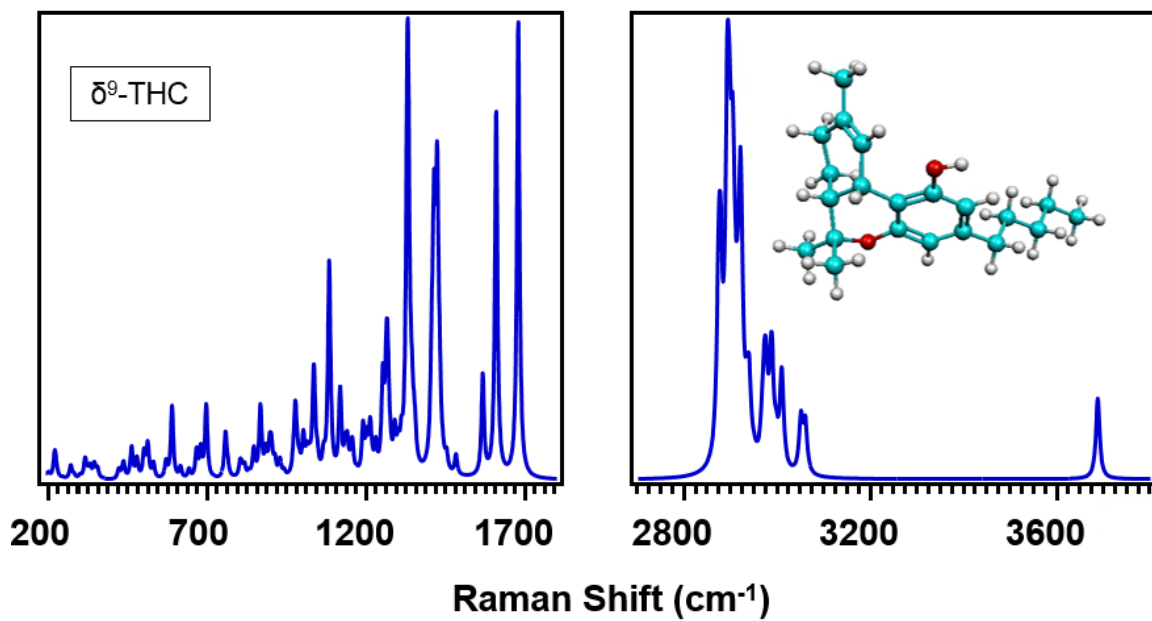


Figure 5.8: Simulated Raman spectrum of δ^9 -THC.

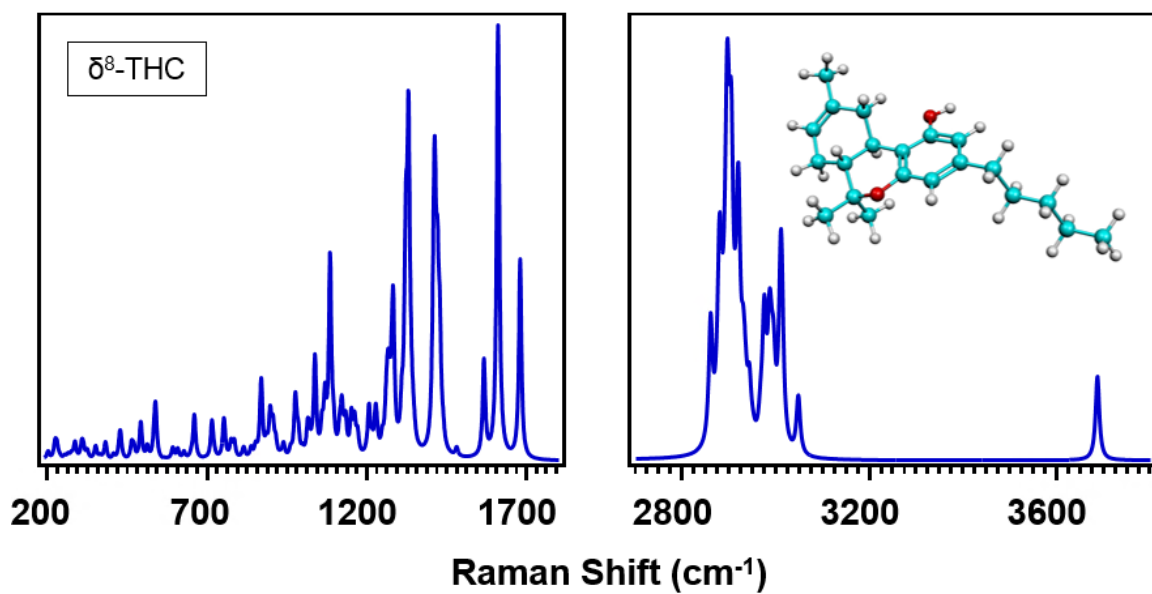


Figure 5.9: Simulated Raman spectrum of δ^8 -THC.

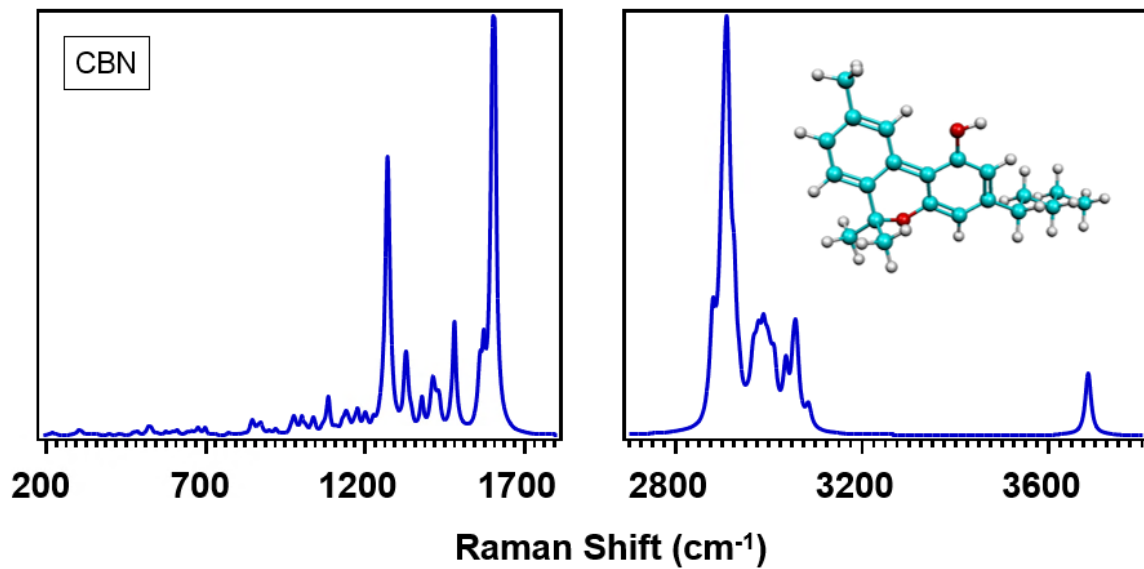


Figure 5.10: Simulated Raman spectrum of CBN.

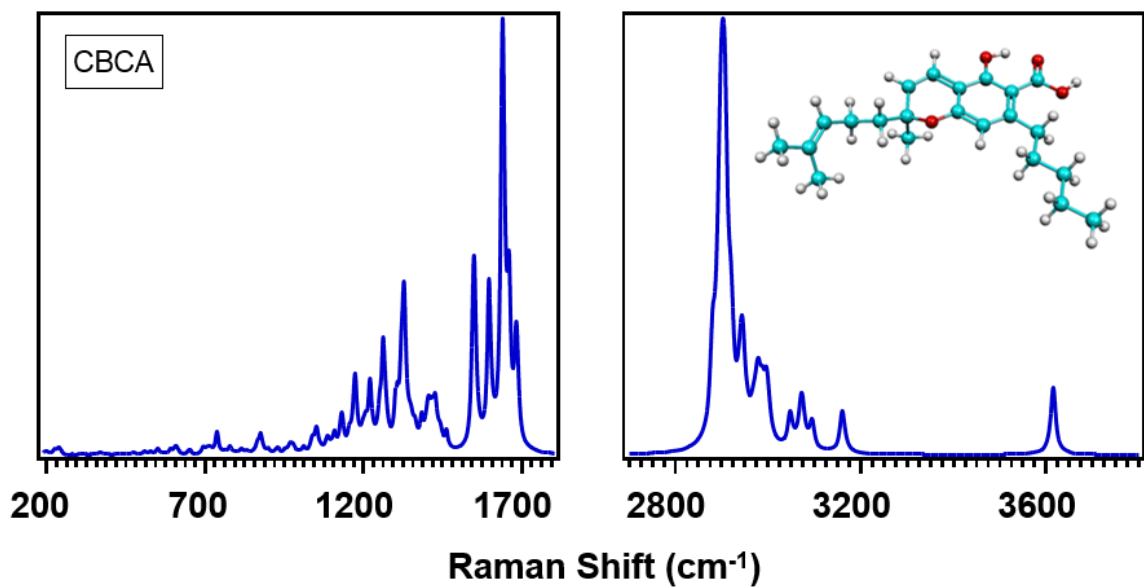


Figure 5.11: Simulated Raman spectrum of CBCA.

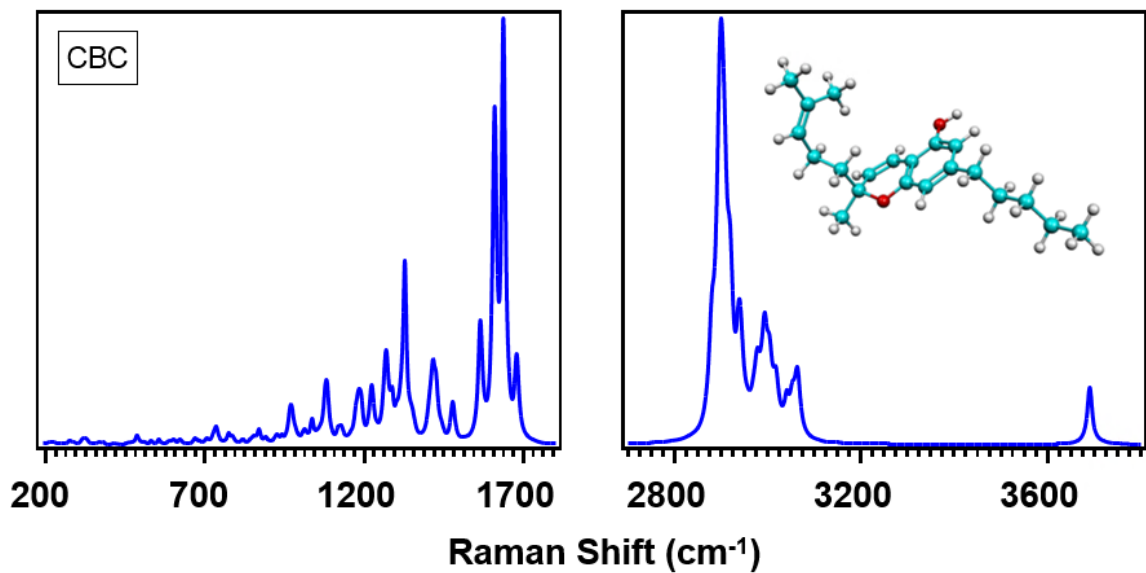


Figure 5.12: Simulated Raman spectrum of CBC.

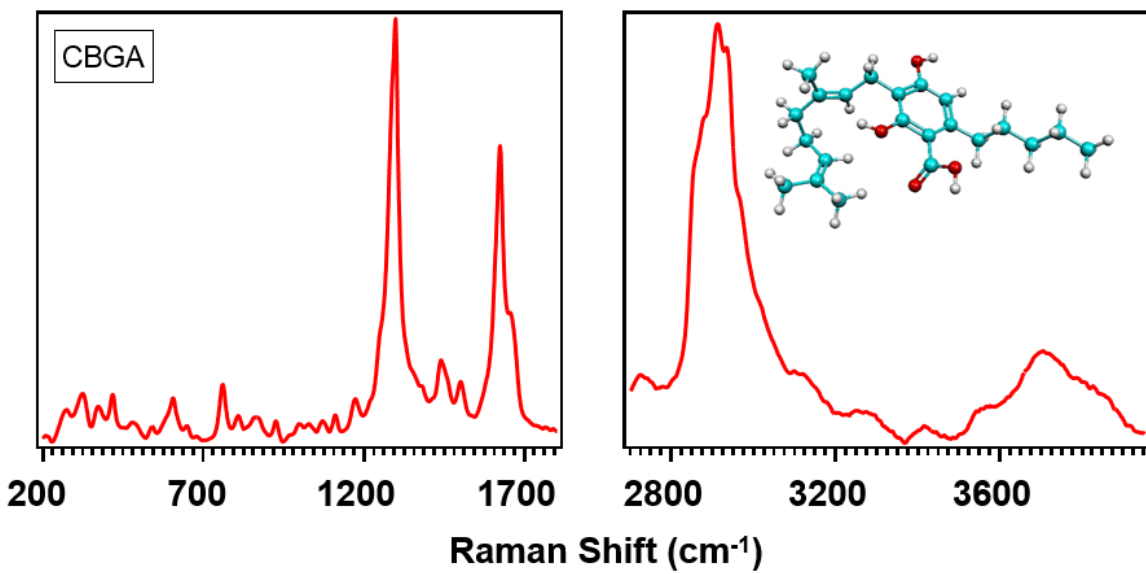


Figure 5.13: Experimental Raman spectrum of CBGA.

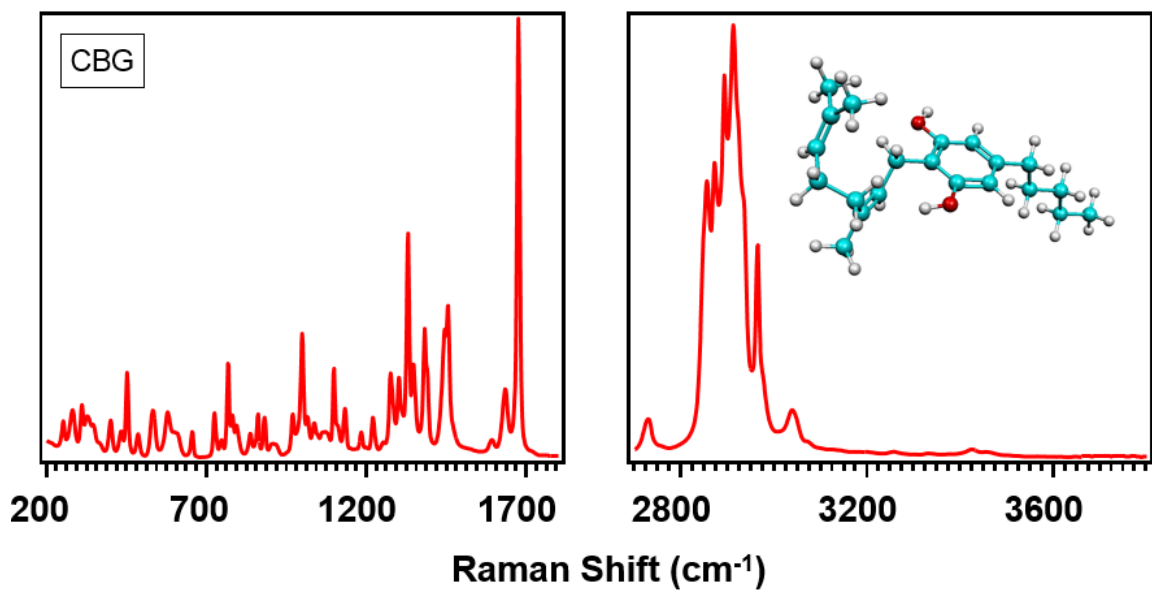


Figure 5.14: Experimental Raman spectrum of CBG.

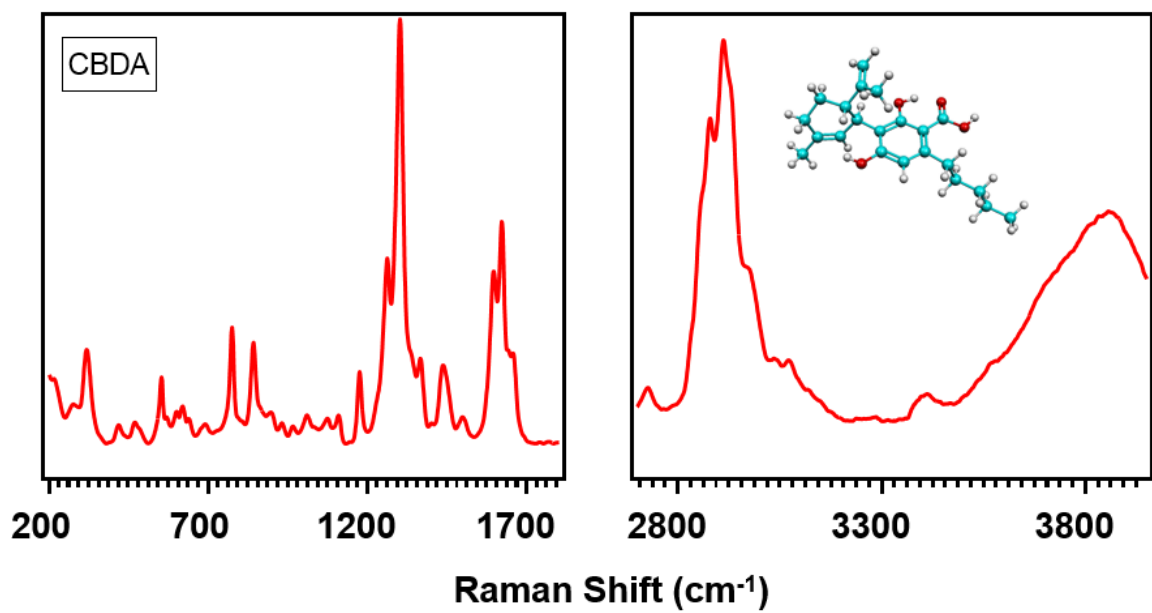


Figure 5.15: Experimental Raman spectrum of CBDA.

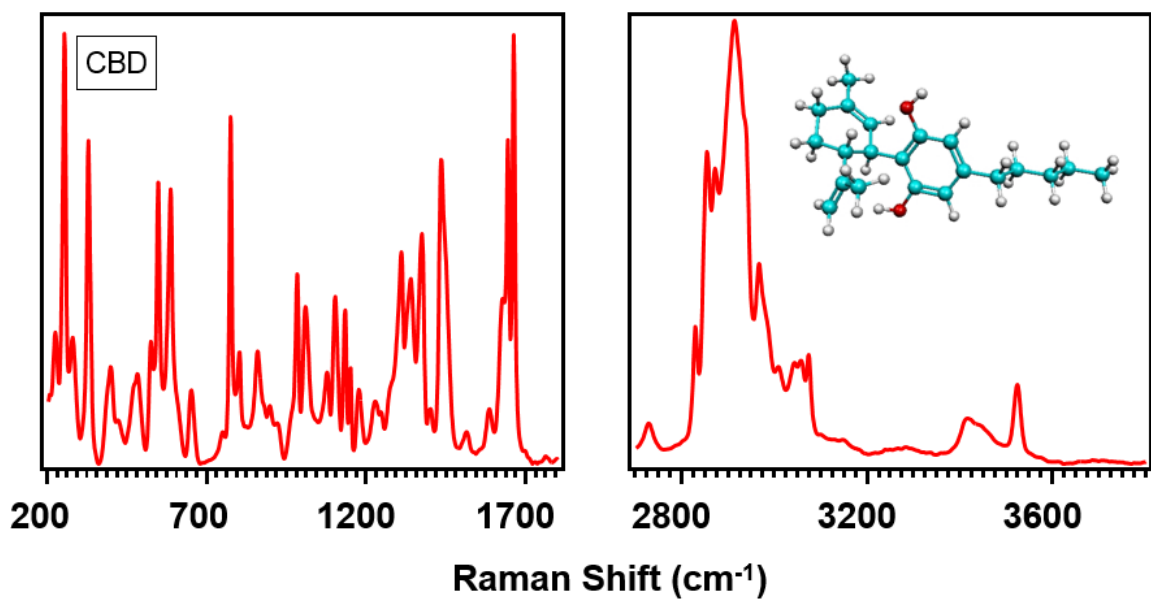


Figure 5.16: Experimental Raman Spectrum of CBD.

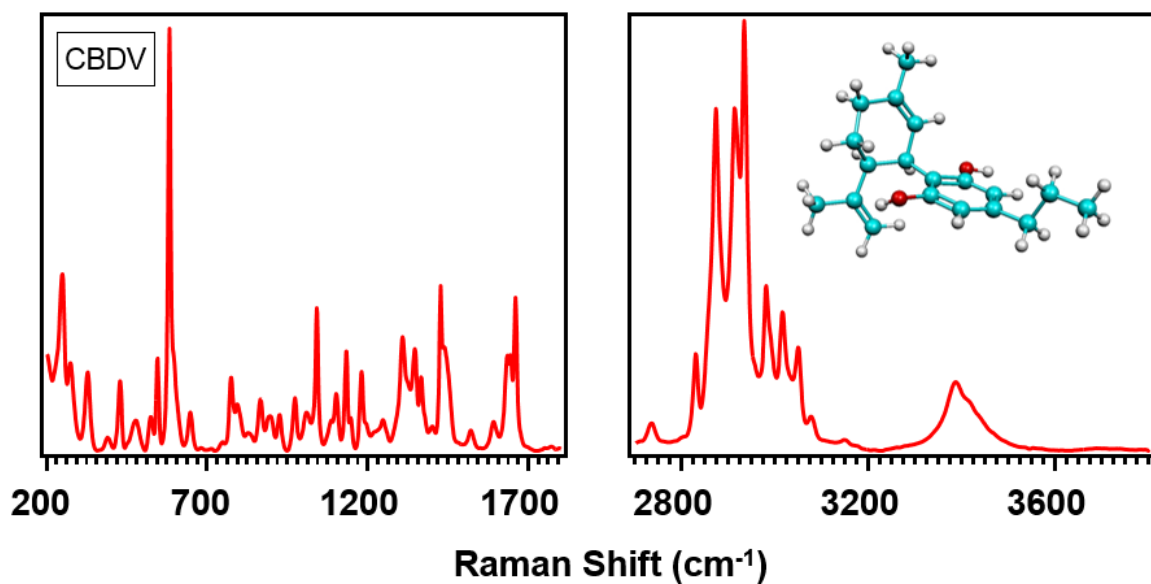


Figure 5.17: Experimental Raman spectrum of CBDV.

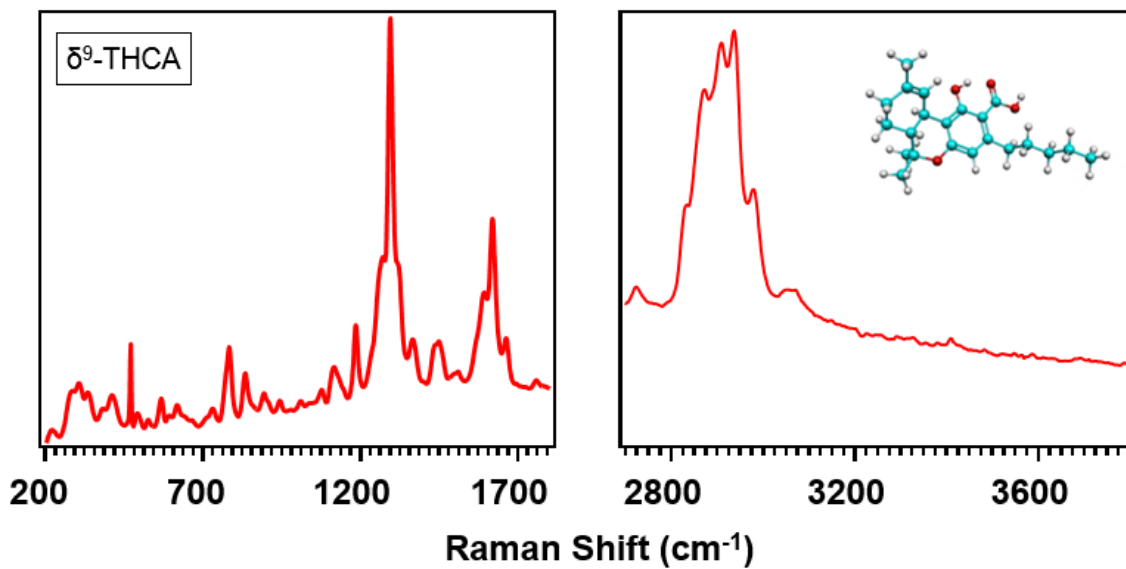


Figure 5.18: Experimental Raman spectrum of δ^9 -THCA.

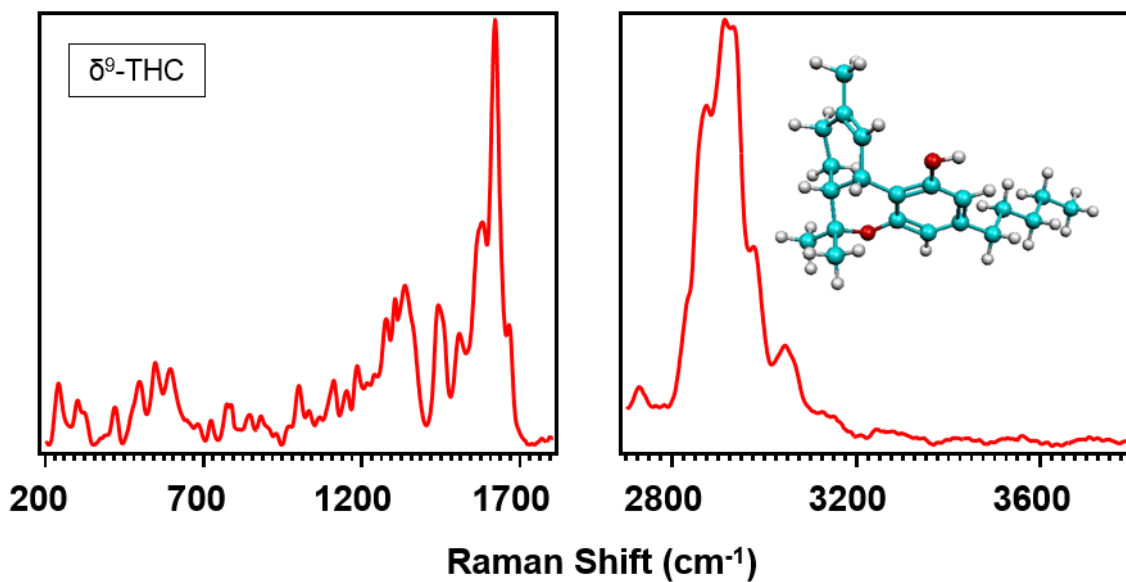


Figure 5.19: Experimental Raman Spectrum of δ^9 -THC.

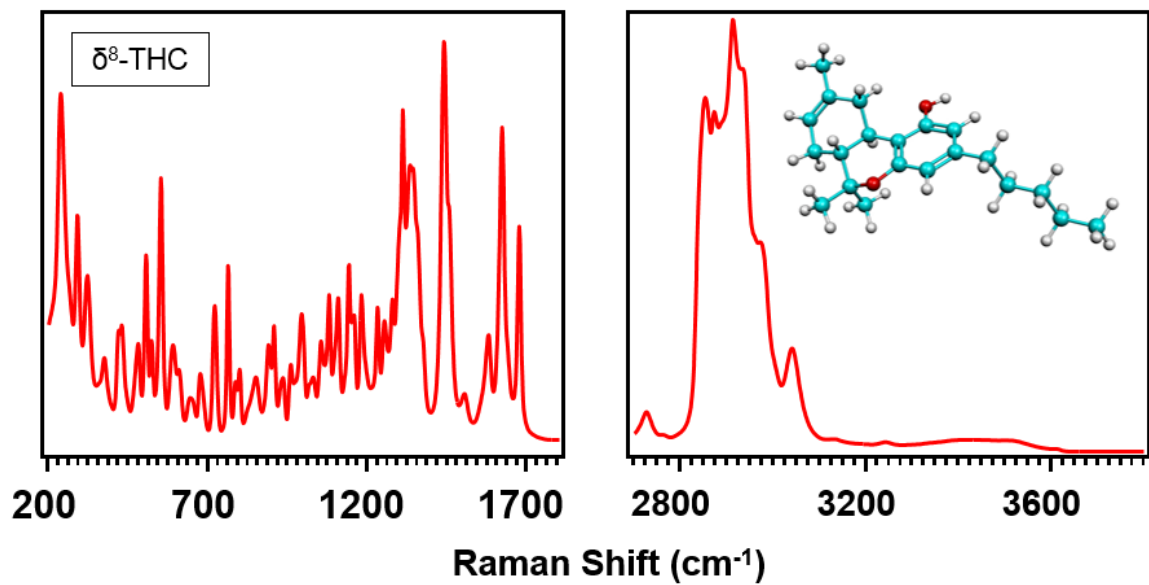


Figure 5.20: Experimental Raman spectrum of δ^8 -THC.

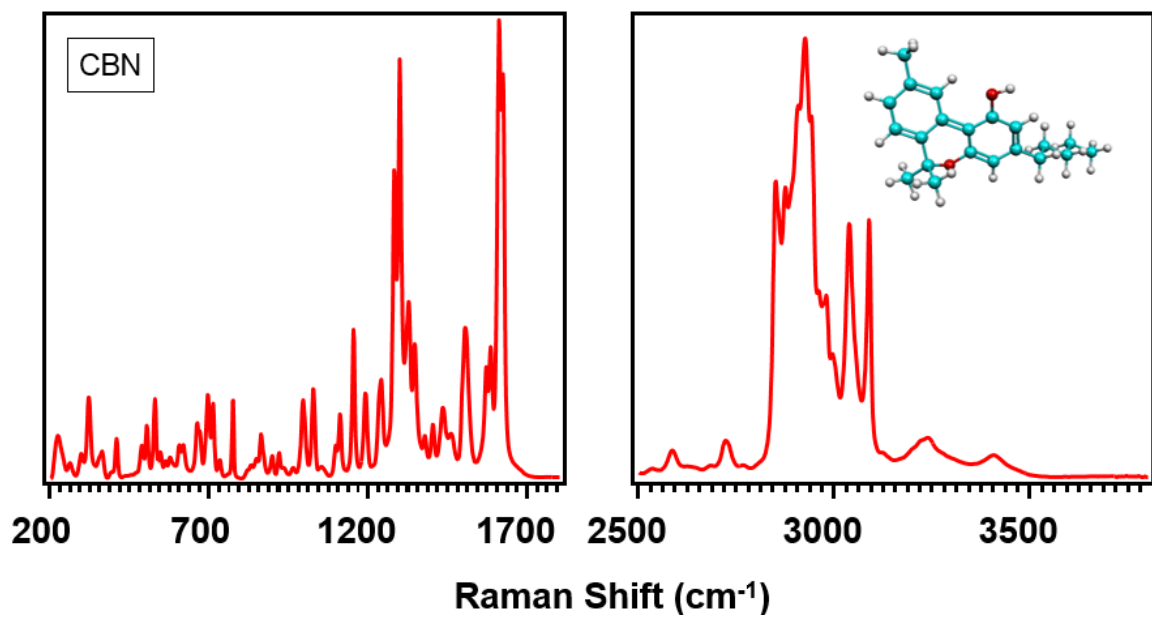


Figure 5.21: Experimental Raman spectrum of CBN.

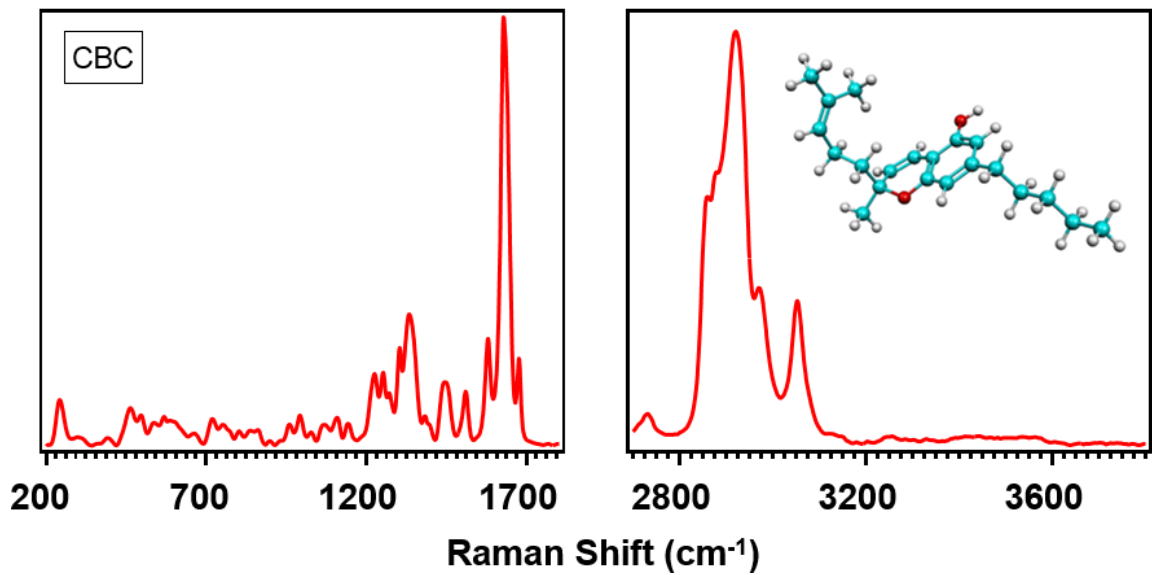


Figure 5.22: Experimental Raman spectrum of CBC.

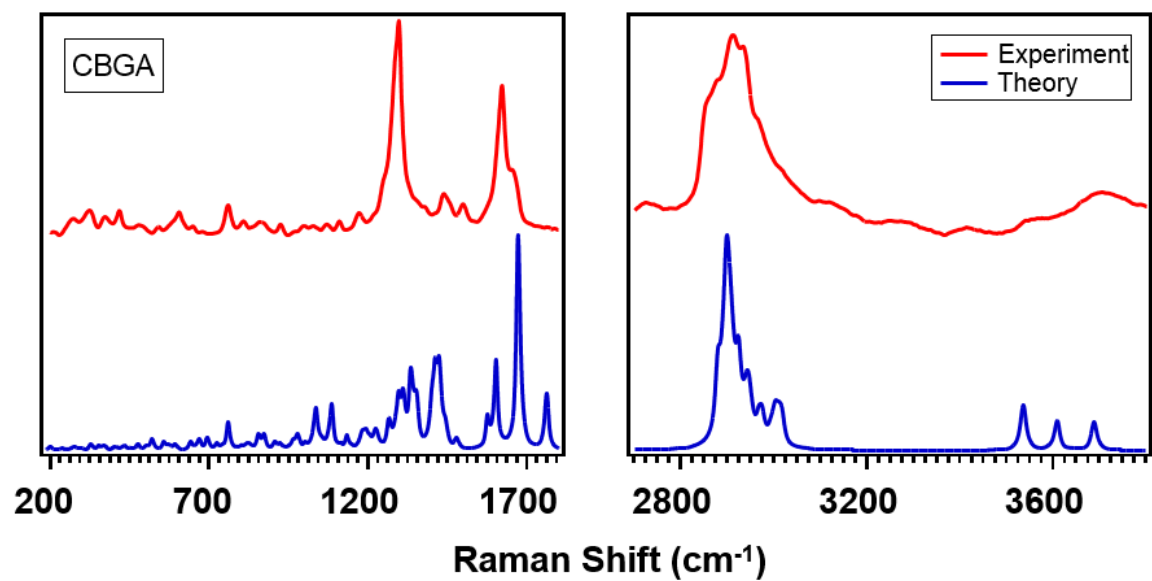


Figure 5.23: Combined Raman spectra of CBGA.

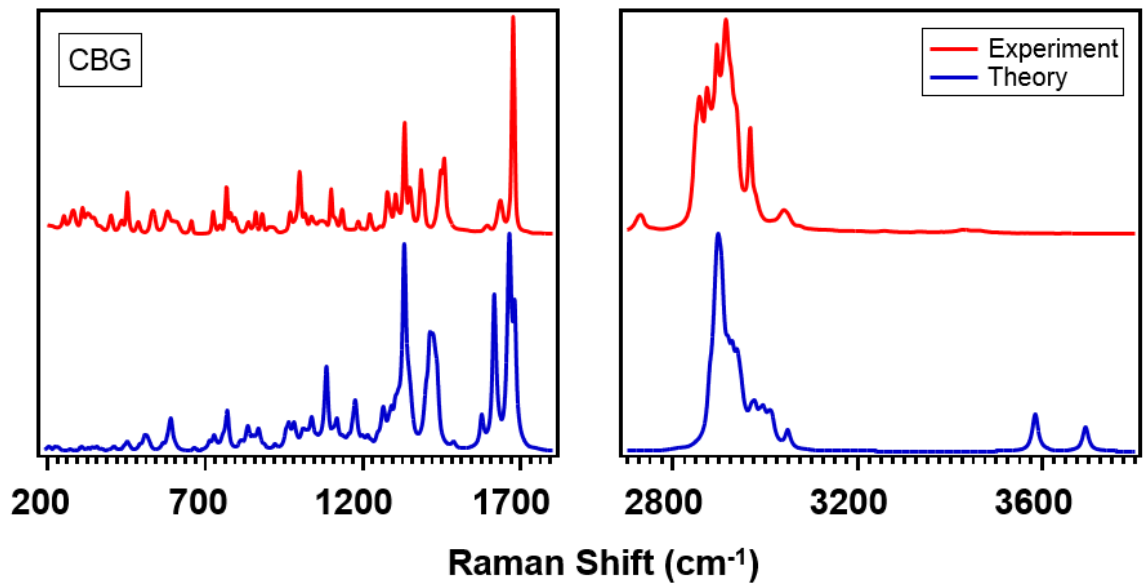


Figure 5.24: Combined Raman spectra of CBG.

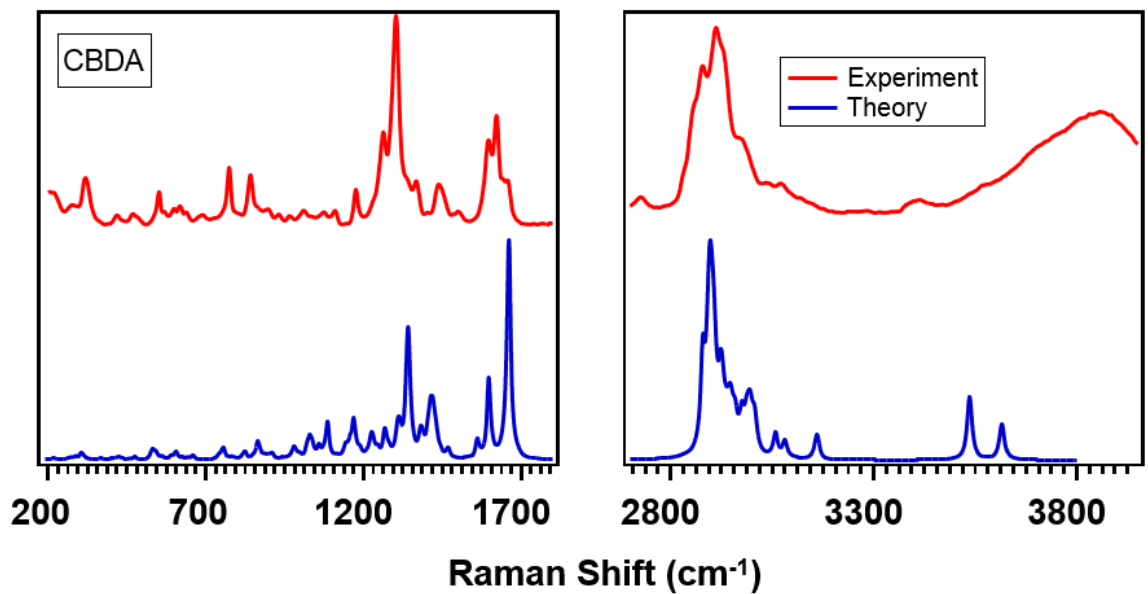


Figure 5.25: Combined Raman spectra of CBDA.

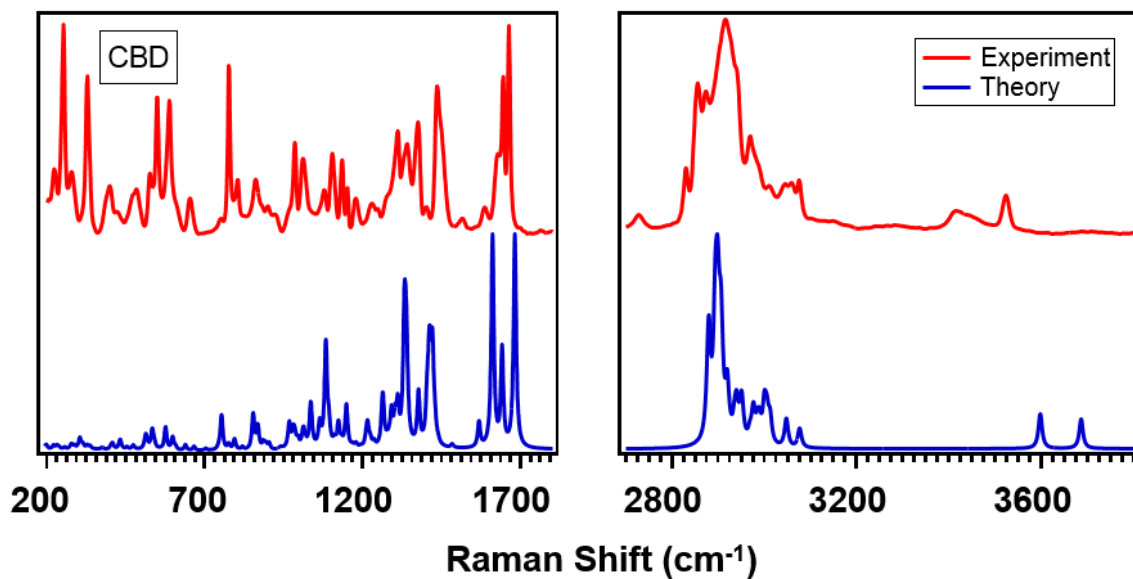


Figure 5.26: Combined Raman spectra of CBD.

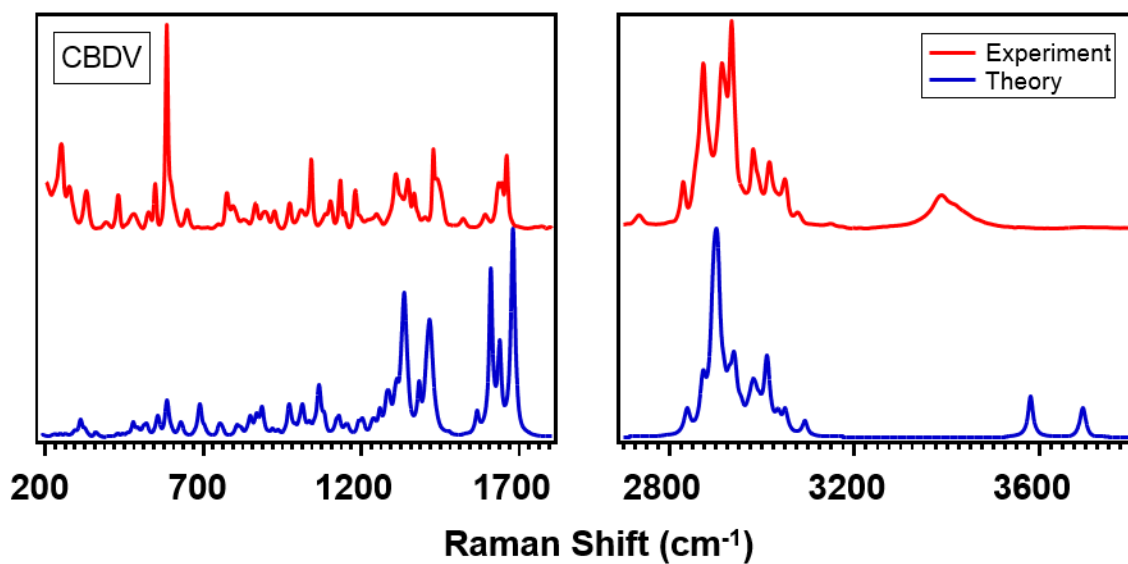


Figure 5.27: Combined Raman spectra of CBDV.

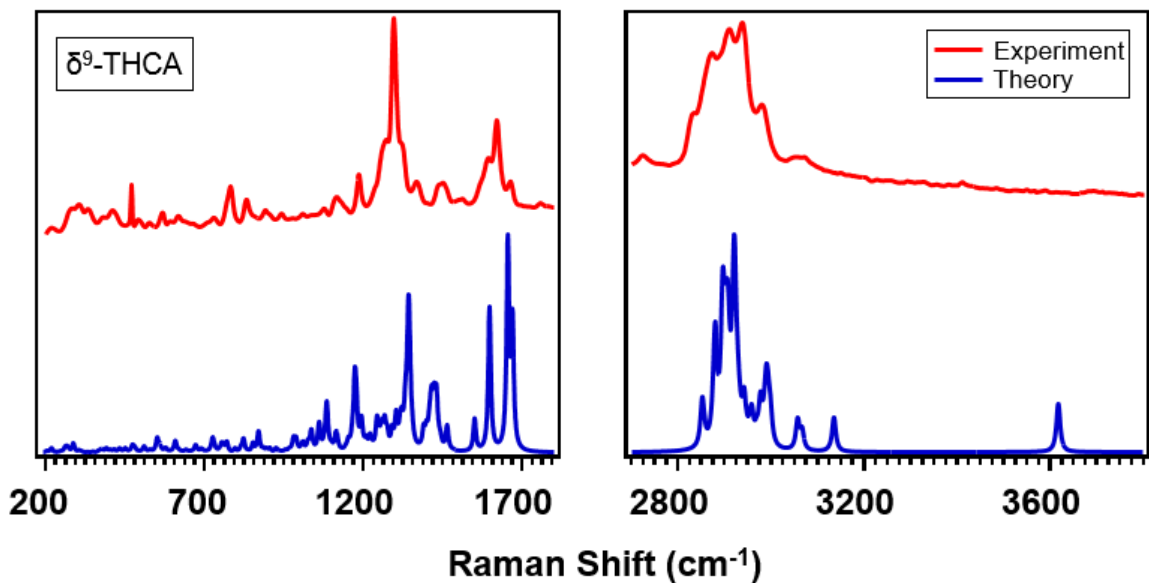


Figure 5.28: Combined Raman spectra of δ^9 -THCA.

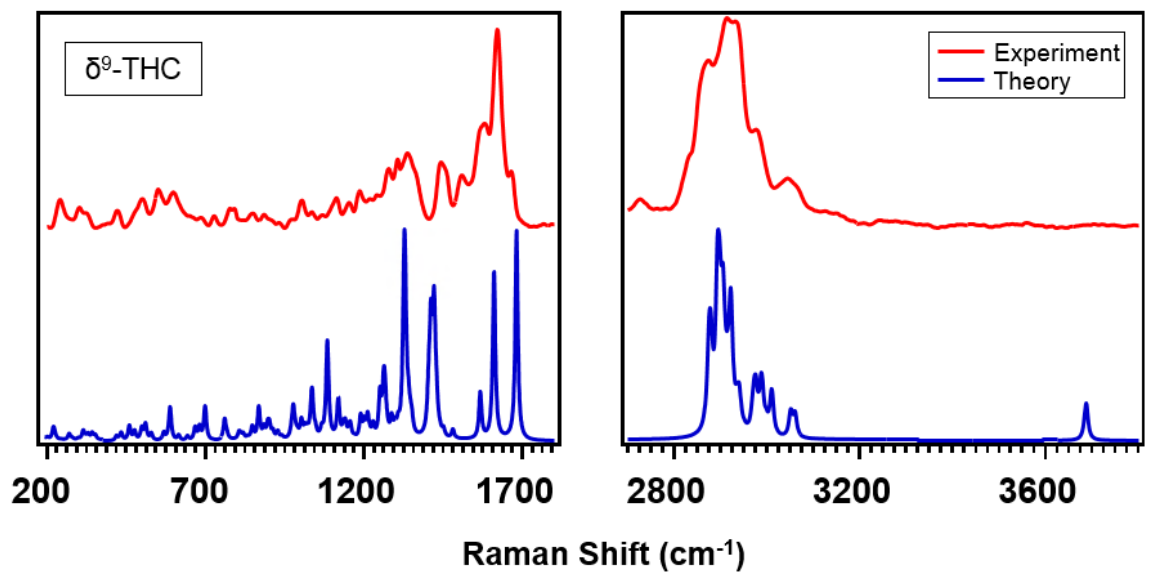


Figure 5.29: Combined Raman spectra of δ^9 -THC.

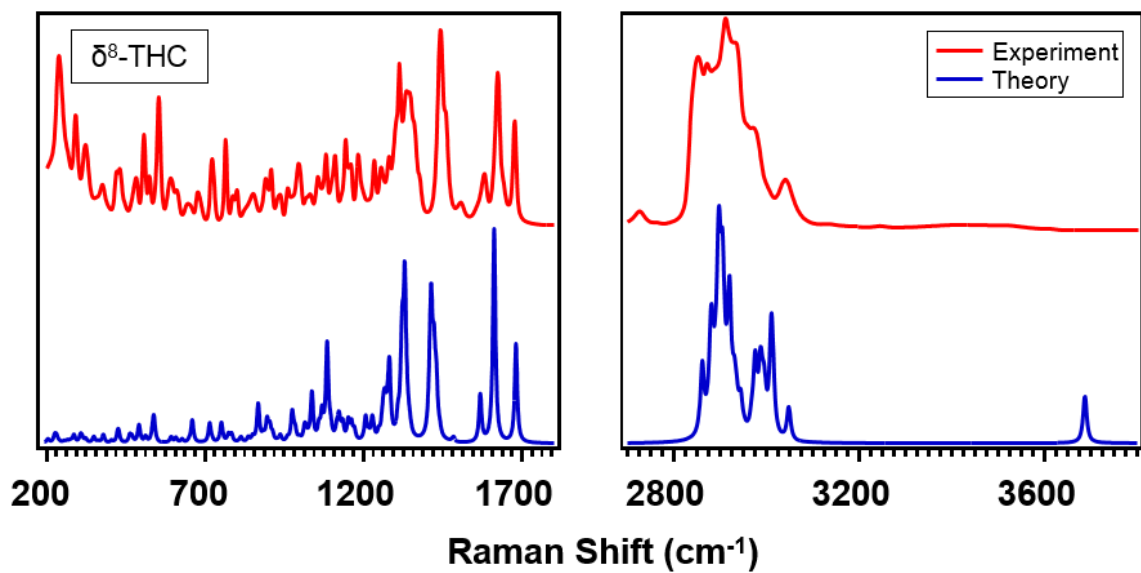


Figure 5.30: Combined Raman spectra of δ^8 -THC.

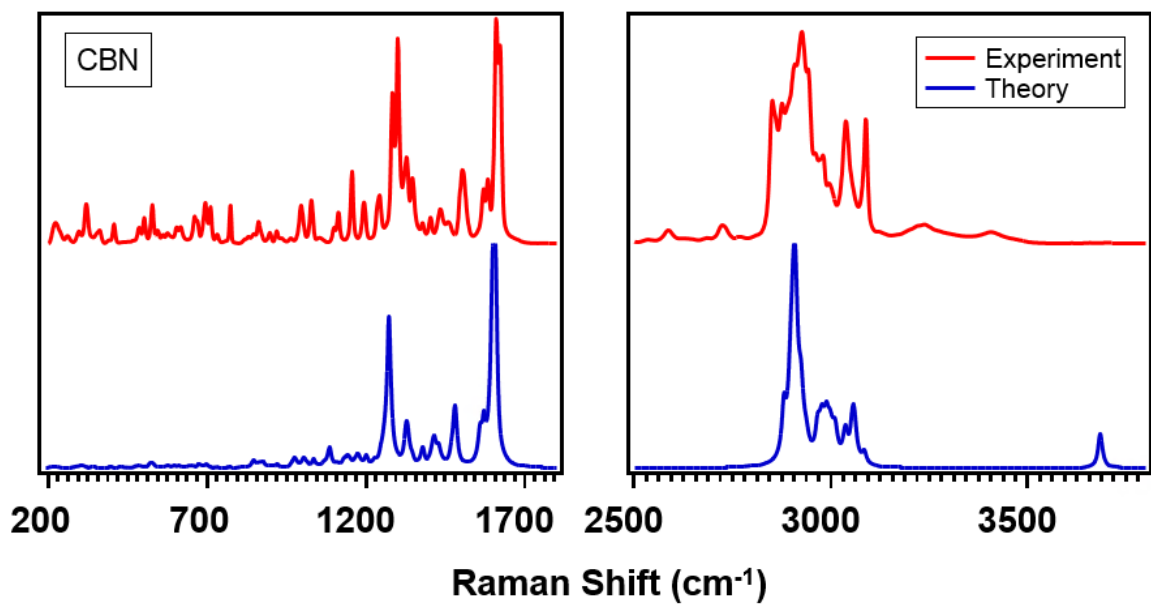


Figure 5.31: Combined Raman spectra of CBN.

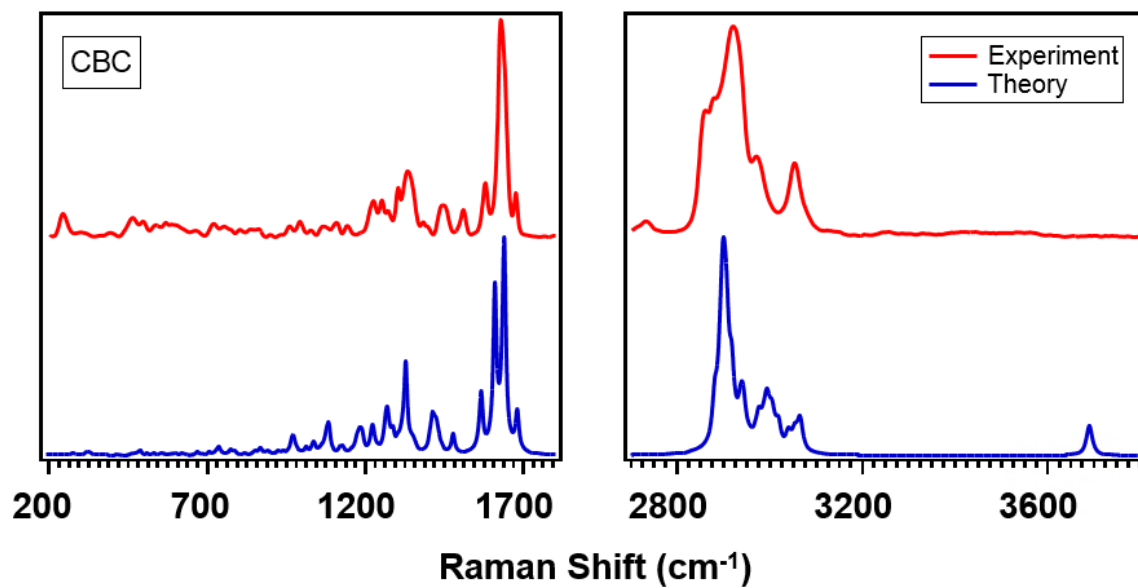


Figure 5.32: Combined Raman spectra of CBC.

CHAPTER VI: DISCUSSION OF RESULTS

6.1 – THE CBG PATHWAY

6.1.1 - CBGA

The experimental spectrum in Figure 5.13 does not demonstrate strong agreement with the simulated spectrum in Figure 5.1, which is especially apparent in Figure 5.23. One of the clearest differences can be seen in the OH stretching region. Specifically, the simulated spectrum predicts three distinct peaks at 3535.5, 3607.7, and 3687.9 cm^{-1} , which can be attributed to the carboxylic OH as well as the two phenolic OH groups. Conversely, the experimental spectrum presents a single broad peak centered at 3704.9 cm^{-1} . This discrepancy likely arises because the calculations used to generate the simulated spectrum only account for a single molecule in isolation. As such, the effects of intermolecular forces cannot accurately be predicted. In essence, there should be three vibrational modes present in the OH region of the experimental spectrum, but band broadening obscures two of the peaks. This result could indicate that the CBGA molecule participates in hydrogen bonding interactions. Further evidence of this conclusion is demonstrated by the blue shift in energy of the OH vibrational modes in the experimental spectrum compared to theory. Whether this intermolecular hydrogen bonding is due to CBGA molecules interacting with each other or with atmospheric water remains unclear at this time.

Furthermore, there is better agreement in the CH stretching region in terms of the Raman shift: the simulated spectrum predicts the most intense peak at

2898.7 cm^{-1} , while in the experimental spectrum it is 2911.3 cm^{-1} . Aside from the slight blue shift in energy, the clearest difference in this region is the lower resolution of the experimental spectrum. While the simulated spectrum predicts five distinct peaks, only two can be discerned from the experimental data. The exact reason for the decrease in resolution cannot be determined from just the spectrum. However, it is possible that the oily nature of the CBGA sample enabled higher rotational freedom in the molecules, which would ultimately cause band broadening and thus less resolution in the vibrational spectrum. There is also the presence of an additional peak at 2723.5 cm^{-1} that is not present in the simulated spectrum. This peak is also present in all other experimental spectra. Potential interference due to ambient room lighting was ruled out, so this peak could simply be a CH stretching mode that has been red shifted from the larger overall band.

Moreover, the fingerprint region, much like the functional group region, does not demonstrate a high degree of agreement between experiment and theory. For instance, the simulated spectrum contains three intense peaks at 1601.9, 1671.3, and 1760.4 cm^{-1} , while in the experimental spectrum there is one distinct peak at 1621.9 cm^{-1} with a shoulder on the right side. As with the OH and CH stretching regions, it is possible that the increased rotational freedom inherent in the oily sample led to the band broadening witnessed in this region of the experimental spectrum. Additionally, the intense peak at 1297 cm^{-1} does not have an immediately clear analog in the simulated spectrum. It is possible that this band represents the peaks at either 1295 or 1308.3 cm^{-1} , but due to its broadness it is difficult to say which one. Aside from these discrepancies, both spectra feature

peaks towards the lower energy end of the fingerprint region that are relatively much less intense than the rest of the peaks. In fact, one vibrational mode in particular has nearly the same Raman shift between experiment (762.1 cm^{-1}) and theory (759.8 cm^{-1}). Overall, comparison between the simulated and experimental spectra of CBGA reveals a less than ideal agreement between the two.

6.1.2 - CBG

Regarding CBG, the only structural difference compared to CBGA is the lack of the carboxylic acid moiety due to thermal decarboxylation. Therefore, one would expect the spectrum of CBG to be very similar to that of CBGA, with the greatest difference occurring in the OH stretching region. Figure 5.2 demonstrates that, at least for the simulated spectrum, this expectation is accurate, as there are only two peaks compared to CBGA's three. However, the experimental spectrum in Figure 5.14 depicts a weaker, less broad band compared to that of CBGA at 3425.4 cm^{-1} . The difference between the two bands is especially prominent in Figure 5.24, as the OH stretching band of CBG is almost indistinguishable compared to that of CBGA. Additionally, rather than experiencing a blue shift, the experimental band undergoes a red shift, thus indicating this vibrational mode is less energetic than what is predicted by theory. Based on these observations, a likely conclusion is that CBG does not participate in hydrogen bonding to the same extent as CBGA. If this is the case, then it is also likely that most of the hydrogen bonding in CBGA occurs through the carboxylic acid moiety.

For the CH stretching region, the simulated band for CBG is visually similar to that of CBGA with only minor differences between them. For one, the most

intense peak is skewed towards the left side of the band for both, the bands are roughly the same width, and both feature a less intense peak towards the right side of the band. The only difference in this last feature is that the peak is narrower and less intense for CBG compared to CBGA. Experimentally, the overall CH stretching band is of comparable width to theory, and the most intense peak is only slightly more energetic than in the simulated spectrum. However, it is skewed more towards the right side of the band, thus suggesting an overall red shift in the entire band. Interestingly, the experimental CH stretching band is more resolved than the simulated band. This result indicates that the different CH vibrational modes in this region are intense enough to appear as distinct peaks on the experimental spectrum, which is not as well predicted in theory. This region is also more resolved when compared to the experimental spectrum of CBGA. In fact, the entire experimental spectrum of CBG has greater resolution than that of CBGA. While this cannot be stated with certainty, it is possible that the increased resolution is due to the more ordered, crystalline nature of the CBG sample compared to CBGA. In essence, molecules are held more in place when in a crystalline arrangement, which restricts their translational and rotational movement. Therefore, the vibrational modes can be better resolved.

In terms of the fingerprint region, there is better agreement between experiment and theory than for CBGA. For instance, the group of peaks occurring before 1700 cm^{-1} is visually similar between both spectra; the most intense peak occurs at the highest energy while the intensities of the other two peaks decrease with energy. The most intense peak also has a Raman shift of 1672.8 cm^{-1} in the

experimental spectrum, while for theory it is slightly higher at 1678.7 cm^{-1} . Compared to CBGA, these peaks are much closer together in both the experimental and simulated spectra. Of note, the highest energy peak in the fingerprint region of CBGA is associated with carbonyl stretching from the carboxylic acid group. Thus, differences in this region can be attributed to the lack of a carbonyl in CBG. Furthermore, the experimental peak at 1329.4 cm^{-1} is in strong agreement with its analogous simulated band at 1328.7 cm^{-1} , with the only major differences being the increased resolution of the experimental spectrum and the appearance of another resolved peak at 1381.3 cm^{-1} . Although the peak at 1454.7 cm^{-1} is considerably blue shifted compared to its analogous simulated peak at 1419.6 cm^{-1} , it is worth noting that both bands are very similar in overall appearance. The major difference between the two is the higher relative intensity in the simulated band. Overall, the agreement between the simulated and experimental spectra is better for CBG than for CBGA. The most notable differences between the spectra of both molecules can possibly be explained by the loss of the carboxylic acid moiety.

6.2 – THE CBD PATHWAY

6.2.1 – CBDA

As part of the CBD biosynthetic pathway, CDBAS converts CBGA into CBDA and CBDVA, which are subsequently decarboxylated into CBD and CBDV respectively. Beginning with CBDA, the simulated spectrum in Figure 5.3 reveals that, as with CBGA, there are three peaks that can be associated with OH stretching vibrations. However, unlike CBGA one of the peaks is closer in energy to the CH

stretching vibrational modes rather than the other two OH modes. The specific Raman shifts of these bands are 3157.8, 3534.4, and 3614.4 cm^{-1} . The highest energy peak is associated with the OH on the carboxylic acid group, while the other two represent the other OH groups in the molecule. Considering the only structural difference between CBGA and CBDA is the cyclization of the terpene tail, it is hard to say with certainty why one OH vibrational mode would be closer in energy to the CH stretching modes. Of note, the lowest energy OH vibrational mode represents the OH that is in closest proximity to the carboxylic acid moiety. It is possible that the calculations are accounting for the possibility of internal hydrogen bonding, but based on the simulated spectrum alone one cannot say for sure that this is the case.

Besides the OH modes, the simulated spectrum features discrepancies in the CH stretching region as well. Specifically, the highest energy band with two peaks is not present in the simulated spectrum of CBGA. Furthermore, there is greater separation, and thus better resolution, between the highest energy peaks of the overall band in CBGA than their counterparts in CBDA. These differences could arise from the cyclization of the terpene tail of CBGA into the monoterpene ring of CBDA, as this conversion would change the nature of some of the CH stretching modes. However, it cannot be said with certainty that this is the cause.

Moreover, the fingerprint region also demonstrates differences between the simulated spectra. Specifically, the vibrational modes around 1700 cm^{-1} differ considerably. For CBGA, the bands corresponding to carbonyl (1760.4 cm^{-1}) and C=C (1671.3 cm^{-1}) stretching modes are well resolved and differ significantly in

energy. On the other hand, these modes are much closer in energy in CBDA, so much so that they overlap in the same band at 1659.3 cm^{-1} . Of note, the C=C stretching modes originate from the double bond in the terpene tail for CBGA and monoterpene ring for CBDA. Since the mode is lower in energy for CBDA, it is possible that cyclization of the terpene tail stabilizes the overall molecule, which could also explain the lower energy of the carbonyl stretching mode. However, based purely on the simulated spectra alone, it cannot be said with certainty that this is why the modes have different energies.

Considering the experimental data, Figure 5.25 demonstrates that, like CBGA, the experimental spectrum is not as resolved as the simulated one. However, it is worth noting that there is stronger agreement between the two in the case of CBDA, though there still are some discrepancies. Similar to CBGA, the greatest difference occurs in the OH stretching region, as there is a very broad and intense band centered around 3855.9 cm^{-1} . Due to the increased broadness and higher intensity of this band compared to that of CBGA, it is possible that CBDA participates in hydrogen bonding to a greater extent than CBGA. Of note, the experimental spectrum demonstrates that, in accordance to theory, there is a separate OH stretching band at 3410 cm^{-1} . Due to its lower intensity and broadness compared to the other band, it is likely that this particular OH group does not participate in hydrogen bonding interactions to the same extent as the other. Regardless, the separation of the OH vibrational modes aligns with theory, and illustrates just one of the spectroscopic differences between CBDA and CBGA.

As with CBGA, the experimental CH stretching band of CBDA was considerably less resolved than the simulated band. Whereas there are eight resolved peaks in the entire simulated band, there are only five in the experimental one. Band broadening is the most likely reason for the decreased resolution, however the root cause of the band broadening is not immediately clear from the experimental data alone. Due to the low resolution of these modes in both molecules, the experimental spectra are not as different in this region as is predicted in the simulated spectra. All that can really be said is that the modes are slightly more resolved for CBDA. However, the spectra are so similar in general appearance in this region that the differences predicted in theory could not be experimentally verified.

Moreover, there also is not as much of a difference between the carbonyl and C=C stretching modes as is predicted in the experimental spectra. For instance, both bands are of comparable width and have the same overall shape, with the most intense peak in the lower energy portion of the band and a peak shoulder on the higher energy side. The only major difference between the two is that most intense peak of the band is split for CBDA, whereas it is continuous in CBGA. Furthermore, both bands have been red shifted and are less resolved than their simulated counterparts. Besides the OH stretching modes, the carbonyl and C=C stretching modes were predicted to be another major difference between the spectra of CBDA and CBGA, so this result is intriguing. As of right now, there is no solid explanation as to why the experimental bands would be so similar. The intense band that occurs just after 1200 cm^{-1} offers another similarity between the

two experimental spectra, with the greatest difference once again being the increased resolution of CBDA compared to CBGA.

In short, the only predicted spectroscopic difference between CBDA and CBGA that could be experimentally verified was the separation in energy of the OH vibrational modes. Perhaps if both experimental spectra were better resolved, the other differences predicted in theory could have been observed.

6.2.2 – CBD

After CBDA is decarboxylated into CBD, Figure 5.4 reveals that the greatest changes in the simulated spectrum occur in the OH and carbonyl vibrational modes, whereas the CH stretching modes are mostly similar. Specifically, the OH vibrational mode associated with the carboxylic acid group is not present. Interestingly, the energy difference between the phenolic OH vibrational modes is not as great in CBD as in CBDA. Recall that in CBDA, the vibrational mode of the phenolic OH in close proximity to the carboxylic acid group was closer in energy to the CH stretching modes than the other OH stretching modes. Thus, it would appear that the presence of the carboxylic acid group had a stabilizing effect on the energy of that particular vibrational mode.

Another result of decarboxylation is the loss of the carbonyl stretching mode. Compared to CBDA, there are four resolved vibrational modes predicted at 1567.5, 1611.2, 1641.6, and 1682.5 cm^{-1} in the simulated spectrum of CBD. The first two correspond to two different breathing modes of the phenol ring, while the other two represent individual C=C stretching modes. Of note, these modes were

also present in the simulated spectrum for CBDA, however the carbonyl and C=C stretching modes were so close in energy that they all appeared to be part of the same peak. However, it seems that in the absence of the carbonyl stretching mode, the two C=C stretching modes have a greater energy difference, and can therefore be better resolved. Why this is the case is not clear, especially considering how far apart in the molecule the carbonyl and C=C bonds are. Additionally, it would also appear that removing the carboxylic acid group causes the higher energy ring breathing mode to have a greater intensity. Based on this result, it is possible that the carboxylic acid moiety hinders that particular ring breathing mode. Except for the differences in C=C and ring breathing modes, the rest of the fingerprint region is virtually identical between CBD and CBDA, though the spectrum for CBD is slightly more resolved.

As one would expect, the simulated CH stretching bands are basically the same between CBD and CBDA. The only major difference between them is the band for CBD is slightly more resolved. For instance, there is greater separation between the two peaks that occur on the higher energy side of the band. Additionally, band splitting not present in CBDA leads to the appearance of two additional peaks in the band for CBD, thus resulting in a total of ten resolved peaks. In experimental spectra, Fermi resonance is a common cause for peak splitting, however it is generally not well predicted in computational studies. Therefore, there is most likely another reason as to why there are more peaks present in the CH stretching band for CBD compared to CBDA, but the theoretical spectrum alone does not reveal what it is.

An examination of Figures 5.16 and 5.26 reveals that the experimental spectrum for CBD has a greater resolution than that of CBDA while highlighting some of the differences between them. Specifically, as was predicted in theory the OH stretching modes of CBD are closer together in energy. Unlike CBDA, these modes are red shifted in energy compared to their simulated analogs. Additionally, there is not nearly as much band broadening present for CBD. In fact, the higher energy OH stretching mode in the experimental spectrum is represented by a distinct peak rather than a broad band. Of note, band broadening still occurs in the lower energy OH vibrational mode, but not to the same extent as in CBDA. This broadening could indicate hydrogen bonding or some other intermolecular interaction at that particular OH. Yet, if this is the case, it is unclear why these interactions would occur at only one OH group and not the other. Further study of the potential for CBD to participate in hydrogen bonding, as well as other intermolecular interactions, would be required to investigate this result.

Regarding the peaks associated with C=C stretching and ring breathing modes, differences between CBD and CBDA as well as between experiment and theory for CBD can be identified. For one, the peaks associated with these modes appear closer together for the experimental spectrum of CBD than in theory, thus resulting in a narrower total width compared to theory. Despite their close proximity, four peaks can be identified, whereas only three were present for CBDA. Specifically, the small peak located to the left of the larger overall band in the spectrum of CBD, which corresponds to a ring breathing mode, is not present in CBDA. Also, the larger band features a shoulder on the left side in the spectrum for

CBD, whereas for CBDA it is on the right side. Based on the results for CBD, the lower energy C=C stretching mode appears to have a greater intensity than the higher energy ring breathing mode, which is the opposite of what was predicted in the simulated spectrum. The reasoning for this observation is not clear, but it demonstrates how it is common for the theoretical calculations to be inconsistent with what is observed experimentally.

Besides the C=C stretching and ring breathing modes, the rest of the fingerprint region highlights a major difference between CBD and CBDA: the majority of the peaks for CBD have high relative intensity and are well resolved, whereas for CBDA the intensity is not as high across the entire region. Of note, this is a significant departure from theory in the case of CBD, as many of the lower energy simulated peaks were predicted to have lower intensities. The most likely explanation for this discrepancy relates to the samples themselves. For CBD, the sample consisted of a singular, pure, highly ordered crystal. On the other hand, the sample for CBDA consisted of a multitude of smaller crystals, though the laser was ultimately focused on an individual crystal. It is possible that, due to its much larger size, the CBD molecules in the crystal were locked more tightly in their crystalline conformation, which could result in the higher intensity vibrations witnessed in the fingerprint region. However, it is difficult to determine if this is truly the case.

Moreover, as the case in the simulated spectra, the experimental spectra of CBD and CBDA are most similar in the CH stretching region. However, there are some minor discrepancies. For one, even though the spectrum of CBD is more

resolved, the overall shape of the CH stretching band is similar to that of CBDA. This is especially the case when comparing the broad, middle peak of the bands, which are virtually identical between the two molecules. Furthermore, the CH stretching modes of CBD are also subject to band broadening. In addition to the most intense peak of the band being much broader in the experimental spectrum compared to theory, there is only a single peak to its immediate right whereas in the simulated spectrum that peak is split. In terms of minor differences, there appears to be an additional resolved peak on the left side of the band for CBD compared to CBDA. However, due to the lower resolution of the CBDA band it is difficult to determine if it would also display that peak.

In short, the greatest differences between CBD and CBDA were observed in the OH stretching region as well as most of the fingerprint region, including the C=C stretching and ring breathing modes. While CBD demonstrated stronger agreement between experiment and theory than CBDA, there were still significant departures from theory present in the experimental spectrum.

6.2.3 – CBDVA

As mentioned previously, CBDVA was not available for study at the time of this work. Therefore, comparisons can only be made between the simulated spectra of CBDVA and CBGA with the caveat that there is no experimental data to support or disprove such comparisons. It can be seen from Figure 5.5 that many of the same spectroscopic differences between CBDA and CBGA also occur in CBDVA. For instance, rather than being closer in energy to the other OH vibrational modes, the one associated with the OH in closest proximity to the carboxylic acid moiety is

similar in energy to the CH stretching modes. Like with CBDA, the optimized structure of CBDVA orients the hydrogen of that particular OH close to the carbonyl oxygen of the carboxylic acid. Therefore, it is possible that the calculations accounted for the possibility of internal hydrogen bonding between those groups, but in the absence of experimental data it cannot be said with certainty that this is the case. Based on the simulated OH vibrational modes, one would expect the experimental spectrum of CBDVA to be similar to that of CBDA, in which there is a smaller broad band close to the CH stretching modes and a broader, more intense band closer to 3800 cm^{-1} . However, the simulated spectra often do not accurately predict experimental observations, so this assumption may or may not be the case.

Like CBDA, the CH stretching modes of CBDVA are predicted to differ from those of CBGA. Specifically, the two highest energy peaks associated with CH stretching in CBDVA are not present in CBGA. Additionally, there are two resolved peaks to the right of the most intense peak in the overall band for CBGA, whereas for CBDVA there is only one. Moreover, the peak shoulder on the left side of the band is lower in energy for CBDVA than for CBGA. As with CBDA, these changes could arise from the cyclization of the terpene tail of CBGA into the monoterpene ring of CBDVA. The effective loss of an ethyl group, and thus several CH stretching modes, in the hydrocarbon tail of CBDVA compared to CBGA could also contribute to some of these differences. Experimentally, one would expect similar results to CBDA in this region. Namely, the experimental CH stretching band would most likely be less resolved than in theory, thus complicating the experimental

comparison between CBDVA and CBGA. However, without any actual experimental data, these statements can neither be supported nor disproven.

Moreover, the clearest predicted deviation from CBGA, besides the OH stretching modes, occurs in the region associated with carbonyl and C=C stretching modes. Although both simulated spectra feature four resolved peaks in this region, the predicted energies and intensities of the peaks differ. For one, the predicted peak for carbonyl stretching in CBDVA has a Raman shift of 1654.6 cm^{-1} , which is considerably lower in energy than in CBGA. In fact, the terpenic C=C stretching mode has greater energy than the carbonyl stretching mode for CBDVA, which is not the case for CBGA. Despite this decrease in vibrational energy, the carbonyl stretching mode of CBDVA is predicted to have greater intensity. Aside from the aforementioned discrepancies, the peaks corresponding to ring breathing modes do not differ significantly, with the only major difference being a greater intensity in the higher energy peak for CBDVA. There is not a solid explanation as to why these results are predicted to occur. Perhaps intramolecular hydrogen bonding between the phenolic OH and the carboxylic acid group decreases the energy of the carbonyl stretching mode below that of the C=C stretching mode. However, given the lack of actual data, neither these predicted results nor the simulated spectroscopic differences between CBDVA and CBGA can be verified.

6.2.4 – CBDV

Figure 5.6 demonstrates that, as a result of decarboxylation, CBDV has one less simulated OH vibrational mode compared to CBDVA. In addition, the OH vibrational mode that was closer in energy to the CH stretching modes in CBDVA

is closer in energy to the other OH vibrational mode in CBDV. Thus, it would appear that the carboxylic acid did have a stabilizing effect on that particular OH vibrational mode, however at this time it cannot be said what specific interaction caused this to occur.

Interestingly, the simulated CH stretching modes of CBDV differ from those of CBDVA more than would be expected. Though, it is important to note that many of these differences could arise from the fact that the peaks in the overall CH stretching band are more resolved for CBDV. Why this is the case is not immediately clear, but it is possible that the increased resolution could be based on the final optimized geometry, which itself could differ from CBDVA simply due to the absence of the carboxylic acid group. For one, the overall CH stretching band of CBDV features two peaks to the left of the most intense peak, whereas for CBDVA there is only one barely resolved peak shoulder. Of note, the band for CBDVA features two peaks to the right of the most intense peak, whereas for CBDV there is only one. Thus, it is possible that, by removing the carboxylic acid group, the first peak to the right of the most intense one for CBDVA increases in intensity. It is currently unclear why this would be the case. Besides this discrepancy, the smaller middle band is resolved into two peaks for CBDV, whereas for CBDVA there is only one. Additionally, the highest energy peak in the overall band for CBDV does not appear in the simulated spectrum for CBDVA. One would not expect as many differences in this region, but it is possible they stem from how the final geometry of CBDV was optimized compared to CBDVA.

In the absence of the carbonyl stretching mode, the two simulated C=C stretching modes have a greater energy difference between them. Specifically, they have Raman shifts of 1636.4 and 1677.9 cm^{-1} compared to 1654.6 and 1685.5 cm^{-1} for CBDVA. Thus, it would appear that removing the carboxylic acid group not only lowers the energy of the C=C stretching modes, but also increases energy difference between them by 10.6 cm^{-1} . Additionally, the higher energy C=C stretching mode is more intense for CBDV, whereas for CBDVA the lower energy mode is more intense. Therefore, in addition to impacting their energies, removing the carboxylic acid group also appears to affect the intensities of the C=C stretching modes. Why this is the case is not clear. Of note, the bands corresponding to ring breathing modes did not change considerably between CBDVA and CBDV, thus suggesting the carboxylic acid moiety had minimal impact on these vibrations.

These predicted spectroscopic changes were largely verified by the experimental spectrum of CBDV. For instance, Figures 5.17 and 5.27 show that, in agreeance with theory, there is not an OH vibrational mode of comparable energy to the CH stretching modes. Instead, there is a broad band with a Raman shift of 3386.8 cm^{-1} that likely accounts for both OH groups present. This band is considerably lower in energy than what was predicted in the simulated spectrum of CBDV. Though it is not certain why this is the case, it is possible that hydrogen bonding or another kind of intermolecular interaction is responsible for both the broadening and decreased energy of the experimentally measured OH vibrational modes compared to theory.

Furthermore, the experimental CH stretching modes of CBDV are more resolved than in theory. For example, there is greater separation between the second and third bands. An interesting departure from theory is that the fourth peak in the overall band is more intense in the experimental spectrum. Despite this minor disagreement, the greater resolution of the experimental CH stretching modes accentuate what was predicted to change between CBDVA and CBDV. Specifically, there are more resolved peaks to the left of the most intense band than there were for CBDVA. Additionally, it is worth noting that the experimental spectra of the acidic cannabinoids thus far were not as resolved as their simulated spectra, especially in the CH stretching region. Therefore, one could predict that there would be an even greater discrepancy between the experimental CH stretching modes of CBDVA and CBDV. However, in the absence of actual experimental data, one cannot simply assume that this will be the case.

Moreover, in spite of decreased intensity of the peaks relative to the simulated spectrum, the experimental spectrum still illustrates that the higher energy C=C stretching mode will have a greater intensity than the lower energy one. Therefore, this predicted difference between CBDVA and CBDV could be verified experimentally. However, because the experimental peaks in this region were closer together than they were in the simulated spectrum, the prediction of the C=C stretching modes being farther apart in energy could not be experimentally verified. Yet, the experimental peaks were red shifted in energy compared to their simulated counterparts (i.e. from 1677.9 to 1658.2 cm^{-1} for the higher energy C=C stretching mode), and are therefore lower in energy than the

peaks in the simulated spectrum for CBDVA. Without experimental data for CBDVA, it cannot yet be said with certainty if the predicted differences between these modes between both molecules occur experimentally.

In short, both the simulated and experimental spectra of CBDV illustrated spectroscopic differences from the simulated spectrum of CBDVA, particularly in the OH, CH, and C=C stretching modes. However, this comparison is inherently weakened by the lack of experimental data for CBDVA, which would have to be collected in a future study in order to verify the observations in this current work.

6.3 – THE THC PATHWAY

6.3.1 – δ^9 -THCA

The third pathway under consideration is the conversion of CBGA into δ^9 -THCA via THCA synthase. From there, δ^9 -THCA is decarboxylated to δ^9 -THC, which is subsequently isomerized to δ^8 -THC and ultimately oxidized to CBN. As was mentioned previously, the conversion of CBGA to δ^9 -THCA leads to an effective loss of one OH functional group; a hydrogen is removed so that the oxygen can bond to an additional carbon group. Therefore, one would expect to see one less vibrational mode in the OH stretching region for δ^9 -THCA. The simulated spectrum in Figure 5.7 demonstrates that this expectation is met, as there are two OH vibrational bands. Like what was observed in the simulated spectra of CBDA and CBDVA, there is a large difference in energy between the OH vibrational modes. Specifically, the carboxylic OH has a Raman shift of 3691.6 cm^{-1} , while for the other OH it is 3047.2 cm^{-1} . Thus, it is possible that δ^9 -THCA also experiences

internal hydrogen bonding between the OH and the carbonyl oxygen, which could explain the decrease in energy of the phenolic OH vibrational mode. However, the experimental spectrum in Figure 5.17 does not reveal if this result occurs experimentally, as there are no discernable peaks in the OH stretching region. One would expect a similar broad band as with CBGA, albeit potentially less broad and intense due to the presence of one less OH group in δ^9 -THCA. The experimental spectrum represents the most resolved data collected for δ^9 -THCA over multiple attempts with several different samples. Ultimately, the hydrogen bonding activities of δ^9 -THCA cannot be determined and compared to CBGA in this work.

Compared to CBGA, there is better agreement between the experimental and simulated CH stretching modes for δ^9 -THCA. For one, the most intense peak in the simulated spectrum occurs at 2918.4 cm^{-1} , while in the experimental spectrum it occurs at 2936.7 cm^{-1} . Despite the blue shift in energy of that specific peak, the entire band appears to have been red shifted. In terms of overall appearance, both spectra contain six major peaks. However, as with CBGA, the experimental spectrum is less resolved, so these peaks are not as well defined as in theory. Because the sample of δ^9 -THCA was crystalline, the composition of the sample itself is likely not the sole cause of the low resolution. Another notable difference between CBGA and δ^9 -THCA in this region occurs at the peak corresponding to the highest frequency vibrational mode. The simulated spectrum of CBGA predicts this peak to be continuous with the overall band at 3003.9 cm^{-1} , while for both the simulated and experimental spectra of δ^9 -THCA it is a separate

peak (3056.2 and 3051.6 cm^{-1} , respectively). Any differences between CBGA and δ^9 -THCA in this region could be attributed to the increase in cyclic rings present in δ^9 -THCA. Essentially, in order for new C-C bonds to form, hydrogens have to be displaced, which would affect the overall CH stretching in the molecule.

Moreover, the fingerprint region of δ^9 -THCA does not show great agreement between experiment and theory. For one, the experimental spectrum is less resolved than the simulated one in this region. Not only is this result consistent with what was witnessed with CBGA, but the decrease in resolution is especially apparent in the peaks occurring before 1700 cm^{-1} . The simulated spectrum predicts four distinct peaks at 1548.5, 1596, 1654, and 1668.2 cm^{-1} . On the other hand, the first peak disappears in the experimental spectrum likely due to band broadening, and the peaks that are present have Raman shifts of 1592.9, 1618.9, and 1662.7 cm^{-1} . Therefore, except for the first experimental peak, the other peaks are red shifted in energy compared to their simulated counterparts. Of note, this trend was also present in CBGA, thus demonstrating some similarity between the two molecules in this respect. Another example of the disagreement between experiment and theory in this region is the experimental peak at 1293.8 cm^{-1} , which is considerably red shifted compared to its simulated analog at 1338.6 cm^{-1} . Of note, this band in particular, as well as the overall fingerprint region, differs significantly from CBGA. These differences likely arise from presence of two additional cyclic rings in δ^9 -THCA compared to CBGA.

6.3.2 – δ^9 -THC

Since the only structural difference between δ^9 -THCA and δ^9 -THC is the removal of the carboxylic acid group, one would expect the two molecules to have similar Raman spectra with the greatest difference originating in the OH stretching region. From the simulated spectrum in Figure 5.8, this expectation is met as there is only one OH vibrational mode present at 3687 cm^{-1} , which is higher in energy than the similar peak at 3615.7 cm^{-1} in δ^9 -THCA. However, as with δ^9 -THCA, Figure 5.18 demonstrates a distinct lack of OH stretching peaks in the experimental spectrum of δ^9 -THC. Therefore, this region is not a viable point of comparison between δ^9 -THCA and δ^9 -THC in terms of experimental data. Additionally, nothing can currently be said about the potential hydrogen bonding interactions of δ^9 -THC.

Better comparisons can be made in the CH stretching region. For one, the simulated spectra of both δ^9 -THCA and δ^9 -THC feature three distinct groups of peaks, with the most noticeable difference being a greater degree of separation between the first and second group for δ^9 -THC. Interestingly, the experimental spectrum of δ^9 -THC is slightly less resolved in this region than δ^9 -THCA, which is the opposite of what was observed in the comparison of CBGA and CBG. Specifically, there are two distinct peaks towards the top of the band in δ^9 -THCA, however these peaks are barely resolved in δ^9 -THC. Despite the slight decrease in resolution, the overall appearance of the experimental band is very similar to δ^9 -THCA. This affirms what would be expected, as the only change in CH bonding

during the conversion to δ^9 -THA is the addition of a hydrogen where the carboxylic acid group was originally bound.

The greatest similarities between δ^9 -THCA and δ^9 -THC, at least as far as theory is concerned, occur in the fingerprint region. Visually, the two spectra are extremely similar with only minor differences between them. Specifically, the peak closest to 1700 cm^{-1} is split in two for δ^9 -THCA, however there is only a single peak in δ^9 -THC. The singular peak in δ^9 -THC reflects the loss of the C=O stretching mode due thermal decarboxylation. This difference aside, the peaks in this portion of the fingerprint region are of similar intensity between the two spectra. Furthermore, the peak at 1420.3 cm^{-1} is shared by both δ^9 -THCA and δ^9 -THC, however it is slightly more intense for δ^9 -THC.

Unfortunately, the comparison in the fingerprint region is not as easy when considering the experimental data. Like δ^9 -THCA, the experimental spectrum of δ^9 -THC is not as well resolved as the simulated one. The easiest comparison can be made for the peaks just before 1700 cm^{-1} . Recall that C=O stretching modes generally occur in this region, so one would expect there to be some difference between δ^9 -THCA and δ^9 -THC in this regard. Interestingly, the only major difference in this region is that the peaks are more intense for δ^9 -THC; both experimental spectra share the same general appearance otherwise and are red shifted compared to their simulated counterparts. An additional difference between the experimental spectra is that the peak at 1293.8 cm^{-1} for δ^9 -THCA is considerably less intense in δ^9 -THC.

Naturally, the lower resolution of the experimental δ^9 -THC spectrum is a major contributor to the poor agreement between experiment and theory. Like with δ^9 -THCA, the data presented here represents the most resolved data after several attempts with different samples. The relatively lower resolution could be due to the inherent instability of the δ^9 -THC molecule. In essence, δ^9 -THC degrades relatively quickly when exposed to intense light and the ambient atmosphere. Thus, it is possible that the sample was actively degrading over the course of the relatively long scan time, which therefore could have contributed to the low resolution of the final spectrum.

6.3.3 – δ^8 -THC

Since the only difference between δ^9 and δ^8 -THC is the position of the double bond in the monoterpene ring, one would expect the two molecules to have nearly identical Raman spectra. A comparison of Figures 5.8 and 5.9 reveals that, as far as theory is concerned, this supposition is mostly supported. There are only a few minor differences between the two spectra. For one, the peak at 3009.6 cm^{-1} in CH stretching band of δ^8 -THC shows an increase in intensity compared to its counterpart in δ^9 -THC. Additionally, in the group of peaks just before 1700 cm^{-1} , the middle is the most intense for δ^8 -THC, whereas for δ^9 -THC the peak with the highest energy is the most intense. Of note, the highest intensity peak corresponds to C=C stretching in the monoterpene ring, while the middle peak corresponds to aromatic ring breathing in the phenolic ring. At this time, there is no solid explanation as to why moving the double bond to the δ^8 position would produce a

more intense ring breathing mode. Other than this discrepancy, the rest of the fingerprint region is similar across both spectra. Furthermore, OH vibrational modes of both spectra are similar in energy: the band has a Raman shift of 3686 cm^{-1} for δ^8 -THC and 3687 cm^{-1} for δ^9 -THC.

Experimentally, Figure 5.20 reveals that unlike δ^9 -THC, δ^8 -THC produces a highly resolved spectrum. An example of the difference in resolution can be seen in the peaks associated with C=C stretching. As discussed previously, these peaks are not well resolved in the spectrum for δ^9 -THC. However, not only are these peaks well resolved in δ^8 -THC, but they also are in near perfect agreement with the simulated bands: the experimental values are 1580.5 , 1622 , and 1676 cm^{-1} , while the simulated values are 1565.6 , 1609.3 , 1677.7 cm^{-1} . Despite the slight blue shift in the first two peaks and red shift in the last, this is one of the few instances where experimental vibrational modes were of comparable energy and intensity to their simulated counterparts. It is possible that, although the change is seemingly minor, moving the double bond in the monoterpene ring to the δ^8 position produces distinct vibrational modes devoid of significant band broadening processes.

Although the experimental CH stretching band of δ^8 -THC has greater resolution than δ^9 -THC, it is still not as well resolved as the simulated spectrum. For instance, Figure 5.30 illustrates that there are eight peaks in the simulated spectrum, whereas in the experimental spectrum only six can be resolved. As with the other cannabinoids, the hydrocarbon tail bound to phenolic ring could

potentially rotate independently of the rest of the molecule. If this is the case, then the rotational freedom of the hydrocarbon tail could explain the band broadening witnessed in the CH stretching region and why it is less resolved than the rest of the spectrum. However, a potential counter to this theory is that the CH stretching band for δ^9 -THC is less resolved than that of δ^8 -THC. Because the two molecules are so similar in structure, one would not expect the hydrocarbon tail of δ^9 -THC to have greater rotational freedom. Since vibrational spectra reveal little about molecular dynamics, it cannot be determined with certainty why the CH stretching of δ^8 -THC is less resolved experimentally than in theory.

Beyond the increased resolution, a key difference between δ^8 and δ^9 -THC is the presence of an OH vibrational mode in the spectrum for δ^8 -THC. Figure 5.20 shows that, compared to theory, the experimental spectrum presents a broad band with a maximum intensity at 3424.1 cm^{-1} . Of note, the intensity of the band is relatively low to the extent it is almost indistinguishable in the combined graph of Figure 5.30. The broadness of the band could indicate the presence of hydrogen bonding interactions through the OH. However, the band is red shifted and has low intensity, so if hydrogen bonding is occurring the extent of these interactions may be low. If a distinct OH vibrational mode was present in the experimental spectrum of δ^9 -THC, further comparisons between the two molecules could be made. Based on how close in energy the simulated bands were, one would expect the experimental OH band of δ^9 -THC to be quite similar to δ^8 -THC. However, as the data has demonstrated thus far, it is common for the experimental data to deviate from what was predicted in theory.

6.3.4 – CBN

Recall that CBN is biosynthesized through the oxidation of δ^8 -THC, resulting in an increased aromaticity of the monoterpene ring. From the simulated spectrum (Figure 5.10), it can be seen that one of the obvious differences between δ^8 -THC and CBN occurs in the region associated with C=C stretching and ring breathing. Recall from both the simulated and experimental spectra of δ^8 -THC that the peaks corresponding to the aforementioned modes were well resolved and easily distinguishable. The same cannot be said for CBN, as there is only one major peak at 1600 cm^{-1} with a barely resolved shoulder on the left side. Essentially, ring breathing in the second aromatic ring replaces the individual C=C stretching mode that was present in δ^8 -THC and adds to the ring breathing mode already present, thus resulting in the singular intense peak observed in that region.

Furthermore, a comparison of the CH stretching region in the simulated spectra reveals another difference between CBN and δ^8 -THC. Specifically, the first peak in the overall band is narrower and less resolved in CBN than in δ^8 -THC. The second peak is also less resolved for CBN than for δ^8 -THC. These differences likely stem from the oxidation reaction that converts δ^8 -THC into CBN. Essentially, in order to add two double bonds to the monoterpene ring, four hydrogens are removed. Thus, the nature of the CH stretching would change at each of the carbons where a hydrogen was removed. Prior to oxidation, the CH stretching mode at two of those carbons would be characterized by an asymmetric stretch where the bond of one hydrogen grows longer while the other shortens during the

course of the vibration. However, when one of the hydrogens is removed, the vibrational mode represents the movement of only one hydrogen as opposed to two. The other two carbons do not have any hydrogens bound after oxidation, so there is an effective loss of two CH stretching modes. These differences in the nature of the vibrations could explain the discrepancies in the CH stretching region between CBN and δ^8 -THC.

Although there are some notable differences, a point of similarity between the simulated spectra occurs in the OH stretching mode. For CBN, the band has a Raman shift of 3683.6 cm^{-1} , while for δ^8 -THC it is 3686 cm^{-1} . In addition to the similarity in energy, both bands have similar intensities. Taking these factors into consideration, one would expect the experimental OH stretching band to be similar to that of δ^8 -THC.

Regarding the experimental data, a comparison of the spectra in Figure 5.31 reveals an overall good agreement between experiment and theory. For instance, the peak associated with ring breathing in the simulated spectrum has a similar appearance and intensity in the experimental one. Besides being slightly blue shifted to 1609.5 cm^{-1} , the experimental band is also slightly more resolved than in theory. This can be concluded from the fact that the most intense peak in the experimental band is split, whereas there is just one peak in the simulated band. The same result occurs for the simulated band at 1270.4 cm^{-1} : the experimental band is blue shifted to 1281.1 cm^{-1} and is split into two distinct peaks. In addition

to these specific bands, the rest of the bands in the fingerprint region with Raman shifts greater than 1200 cm^{-1} follow this pattern.

Unlike what was observed with other cannabinoids, the high resolution of the experimental spectrum also extends into the CH stretching region. Specifically, although the first peak in the overall band is broader in the experimental spectrum, more resolved peaks can be identified than in the simulated spectrum. Additionally, greater peak separation can be observed towards the higher energy side of the band. However, a key difference is that unlike the simulated spectrum, there is not a clearly defined middle peak in the experimental band. It is possible that the broadening of the first band could have prevented the middle band from being clearly resolved in the spectrum. Regardless, the results demonstrate there is weaker agreement between experiment and theory for the CH stretching modes than others. Another interesting departure from theory demonstrated in the experimental spectrum is the presence of an additional peak similar to the one present in every experimental spectrum, which occurs before the CH stretching band. This additional peak, which has a Raman shift of 2534.8 cm^{-1} , does not have a corresponding band in the simulated spectrum. Therefore, it is difficult to determine whether this peak is actually characteristic of CBN, or it stems from the presence of an impurity in the sample.

Moreover, the experimental spectrum also differs from theory in the OH stretching region. Whereas the simulated spectrum features a narrow band with only one peak, the experimental spectrum features a broad band with two peaks. In addition to the broadness of the band, it has also been considerably red shifted

compared to its simulated counterpart. A red shift of this degree could indicate that CBN does not participate in considerable hydrogen bonding interactions. Instead, other as of yet unknown intermolecular interactions could be responsible for the band broadening. The other issue is the splitting of the band into two peaks. If both peaks truly represent OH stretching, then it is possible that Fermi resonance, which is generally not well predicted in theory, could be the cause. However, this also cannot be stated definitively.

Based on the results presented in the experimental spectrum, most of the differences between CBN and δ^8 -THC predicted in theory were represented in reality. For one, the experimental spectrum depicted that, in accordance with theory, the presence of a second aromatic ring produced a more intense peak associated with ring breathing, thus replacing the C=C stretching vibrational mode. Additionally, the experimental CH stretching region of CBN, though slightly different than theory, is markedly different from that of δ^8 -THC. Specifically, the two peaks towards the higher energy side of the band in CBN are not present in δ^8 -THC. While it cannot be stated as fact, this result supports the theory that the removal of hydrogens during the oxidation reaction has an effect on the CH stretching band. Moreover, although the experimental OH stretching bands of CBN and δ^8 -THC are both broad, there is one continuous band for δ^8 -THC as opposed to two in CBN. Again, based purely on the data the reason for this discrepancy is not clear, but it serves as a reminder that what is observed in reality does not always align with theoretical expectations.

6.4 – THE CBC PATHWAY

6.4.1 – CBCA

Since CBCA was not available for study, comparisons can only be made between the simulated spectra of CBCA and CBGA. Figure 5.11 shows that, as would be expected based on the structure of CBCA, its simulated spectrum contains two OH vibrational modes compared to CBGA's three. With a Raman shift of 3158.9 cm^{-1} , the phenolic OH vibrational mode, like with the other acidic cannabinoids other than CBGA, is closer in energy to the CH stretching modes. Again, the most likely explanation is that the orientation of the hydrogen of the phenolic OH close to the carbonyl oxygen could lead to internal hydrogen bonding, and thus a stabilization of that vibrational mode. Because this observation was experimentally verified for CBDA, one would expect the same to occur for CBCA. However, in the absence of experimental data, one cannot assume that this will be the case.

Only minor spectroscopic changes are predicted to occur in the CH stretching region upon the conversion of CBGA into CBCA. Specifically, the band with three peaks in between the phenolic OH and the other CH stretching modes is not present in the simulated spectrum of CBGA. Additionally, the band at 2976.8 cm^{-1} for CBCA is not as resolved as its counterpart in the simulated spectrum of CBGA. Based solely on the simulated spectrum, the reason for these differences cannot be determined with certainty. However, it is possible that these differences arise from the increased cyclization of CBCA compared to CBGA. In essence, the bonds formed from converting CBGA into CBCA could affect the CH stretching

modes, thus leading to the differences between the simulated spectra. However, the lack of actual experimental data for this molecule means this conjecture cannot be validated as of yet.

Moreover, the region associate with carbonyl, C=C, and ring breathing vibrational modes demonstrates clear differences between CBGA and CBCA. For one, the carbonyl stretching mode of CBCA is predicted to have less energy than that of CBGA (1657 vs 1760.4 cm^{-1}). Therefore, unlike CBGA the carbonyl stretching mode is predicted to have less energy than the C=C stretching mode of the double bond in the terpene tail for CBCA. There are also five resolved peaks in this region of the simulated spectrum of CBCA, whereas for CBGA there are only four. This is mainly due to the fact that the C=C stretching modes are predicted to be further apart in energy for CBCA than they are for CBGA, which itself could be a result of the structural difference between the two molecules. For CBGA, the C=C stretching modes come from the two double bonds present in the terpene tail. Because each of these double bonds have similar groups bonded to them, it makes sense that their vibrational energy levels would be almost the same. On the other hand, the double bonds representing the C=C stretching modes of CBCA do not have similar atom groups bonded to them, which would contribute to their larger difference in energy. Moreover, the other major difference in this region is the higher intensity of the lower energy ring breathing mode of CBCA compared to CBGA. The root cause of these differences cannot be determined based purely on the simulated spectra, however the most likely reason involves the structural differences between the two molecules.

6.4.2 – CBC

From Figure 5.12, it is clear that the simulated spectrum of CBC only has one peak corresponding to an OH vibrational mode compared to the two of CBCA. This makes sense considering the decarboxylation of CBCA into CBC effectively removes one OH vibrational mode. Like with most of the other decarboxylated cannabinoids, removal of the carboxylic acid moiety appears to correlate with an increase in energy of the other OH vibrational mode. Therefore, it would seem that, whether due to internal hydrogen bonding or some other interaction, the carboxylic acid group stabilized and thus decreased the energy of the phenolic OH vibrational mode. However, this cannot be stated with absolute certainty.

Furthermore, the simulated CH stretching modes of CBC are not drastically different from those of CBCA, which is expected given the structural similarity between the two molecules. The only notable differences occur in the two bands to the right of the most intense one. For CBC, the less energetic of these two has three resolved peaks, whereas there are only two for CBCA. Conversely, the higher energy band has two resolved peaks for CBC compared to the three of CBCA. Of note, these differences are only minor, as the overall CH region is very similar between the two molecules. These minor differences could be the result of the addition of a CH vibrational mode on the phenolic ring due to the loss of the carboxylic acid group, but this cannot be said for sure.

Moreover, due to the loss of the carboxylic acid group, the region associated with carbonyl, C=C, and ring breathing vibrational modes has four peaks for CBC compared to the five of CBCA. Unlike what was observed with other cannabinoids,

there does not appear to be an appreciable effect on the intensity and energy of the C=C vibrational modes upon removal of the carboxylic acid group. Instead, the major changes occur in the peaks associated with the ring breathing modes. Compared to CBCA, the lower energy ring breathing mode of CBC decreases in intensity while the opposite occurs for the higher energy ring breathing mode. Based on these simulated results, it seems that removing the carboxylic acid group has more of an impact on the ring breathing modes than the C=C stretching modes.

Even though the experimental spectrum of CBC, shown in Figures 5.22 and 5.32, is less resolved than the simulated spectrum, it mostly validates the spectroscopic differences predicted to occur between CBCA and CBC. However, the experimental results were not as clear for the OH vibrational mode. It is possible that, like δ^8 -THC, there is a very broad and relatively weak band spanning 3200-3600 cm^{-1} , but it is unclear if this is an actual band or if it is simply instrumental noise. If it is a band, its broadness is an intriguing result that could indicate hydrogen bonding interactions. Because there is no experimental data for CBCA, it is as of yet unknown how the actual OH stretching modes of CBCA would compare to that of CBC. However, from the experimental spectra of the other acidic cannabinoids, it is possible that the OH stretching band of CBCA would be broad like with CBC, however the relative intensity and energy would likely be much greater.

Despite the decreased resolution of the experimental CH stretching modes, specific differences can be identified between them and the simulated modes of both CBC and CBCA. For one, the most intense peak of the overall experimental

band has two distinguishable shoulders on its left side, whereas for both CBC and CBCA there is only one. This could potentially be due to a higher observed intensity in the peak located to the right of the most intense band in both CBC and CBCA. Yet, due to the broadness of the experimental CH stretching modes compared to theory, it is difficult to definitively determine if this is the case. Furthermore, the band located at 3051.7 cm^{-1} in the experimental spectrum only has one resolved peak, whereas CBC and CBCA have two and three, respectively. While the middle band in this region was clearly resolved for the simulated spectra of CBC and CBCA, this was barely the case for the experimental spectrum of CBC. If the resolution could be improved, it is possible that the CH stretching region of the experimental spectrum of CBC would not differ as much from theory. If experimental data for CBCA could have been collected, it is possible that, based on the results of the other acidic cannabinoids, the CH stretching region would not be as resolved, thus making comparison to CBC more complicated.

Perhaps the best agreement between experiment and theory for CBC, at least in terms of energy and intensity, occurs for the C=C and ring breathing modes. As can be seen in Figure 5.32, the higher energy C=C and lower energy ring breathing modes are of comparable energy and intensity to their analogs in the simulated spectrum. The only major discrepancy in this region is that, whether due to band broadening or a smaller energy gap between them, the higher energy ring breathing and lower energy C=C stretching modes are not distinctly resolved in the experimental spectrum. Regardless of this minor inconsistency, the less energetic ring breathing mode appears to be less intense than the more energetic one, thus

experimentally validating one of the differences between the simulated spectra of CBC and CBCA. Whether or not the experimental spectrum of CBCA would also differ significantly from that of CBC in this region remains to be seen.

In short, the experimental spectrum of CBC demonstrated good agreement to theory, and thus validated some of the spectroscopic differences from CBCA predicted by the simulated spectrum.

CHAPTER VII: CONCLUSIONS AND FUTURE WORK

To conclude, the data presented in this work represents the most resolved experimental and simulated spectra that could be produced for each cannabinoid. The derivatives of CBGA often displayed higher resolution in the experimental spectra than CBGA itself, which is most likely attributable to physical composition of the samples. The overall agreement between the experimental and simulated spectra was good, however there were certain vibrational modes where the agreement was not as strong. This was especially evident for the OH stretching vibrational modes, which were either red shifted or blue shifted in energy compared to what was predicted in the simulated spectra. Regardless, the most evident spectroscopic changes were observed in this region, especially when transitioning from an acidic to a decarboxylated cannabinoid. Therefore, the OH stretching region could be a good probe for decarboxylation reactions. Although not as evident, spectroscopic differences were also identified in the C=C stretching and ring breathing modes, which were mostly attributed to the loss of a C=O stretching mode due to decarboxylation.

This present work was largely limited by its overall scope. Given the complexity of both their simulated and experimental spectra, the number of cannabinoids included in this study prevented an in depth discussion of the peak to peak differences between each cannabinoid and between experiment and theory. Future works could focus on fewer cannabinoids at a time, thereby allowing more in depth discussion of the spectra. If they become more available in the future, experimental spectra for CBDVA and CBCA should be obtained for more

accurate comparison to the experimental spectra of CBDV and CBC. Moreover, future works should investigate hydrogen bonding interaction in the acidic cannabinoids, especially if internal hydrogen bonding between the phenolic OH and carbonyl oxygen actually occurs, and how it affects vibrational energy. Further computational studies could investigate the different isomeric forms for each cannabinoid to determine if there is an appreciable difference in their simulated spectra.

CHAPTER VIII: REFERENCES

1. Aizpurua-Olaizola, O., Omar, J., Navarro, P. *et al.* Identification and quantification of cannabinoids in *Cannabis sativa L.* plants by high performance liquid chromatography-mass spectrometry. *Anal Bioanal Chem* **406**, 7549–7560 (2014).
2. ElSohly, M. A. and D. Slade (2005). "Chemical constituents of marijuana: The complex mixture of natural cannabinoids." *Life Sciences* **78**(5): 539-548.
3. Fellermeier M, Zenk MH. Prenylation of olivetolate by a hemp transferase yields cannabigerolic acid, the precursor of tetrahydrocannabinol. *FEBS Lett.* 1998 May 8;427(2):283-5.
4. Degenhardt, F., F. Stehle, et al. (2017). Chapter 2 - The Biosynthesis of Cannabinoids. *Handbook of Cannabis and Related Pathologies*. V. R. Preedy. San Diego, Academic Press: 13-23.
5. Helander, A., M. Johansson, et al. (2022). "Analytical and medico-legal problems linked to the presence of delta-8-tetrahydrocannabinol (delta-8-THC): Results from urine drug testing in Sweden." *Drug Testing and Analysis* **14**(2): 371-376.
6. Johnson-Arbor, K. and S. Smolinske (2021). "The current state of delta-8 THC." *The American Journal of Emergency Medicine*.
7. Tzadok, M., S. Uliel-Siboni, et al. (2016). "CBD-enriched medical cannabis for intractable pediatric epilepsy: The current Israeli experience." *Seizure* **35**: 41-44.
8. Devinsky, O., M. R. Cilio, et al. (2014). "Cannabidiol: Pharmacology and potential therapeutic role in epilepsy and other neuropsychiatric disorders." *Epilepsia* **55**(6): 791-802.

9. Szaflarski, J. P., & Bebin, E. M. (2014). Cannabis, cannabidiol, and epilepsy—from receptors to clinical response. *Epilepsy & Behavior*, *41*, 277-282.
10. Eggers, M. E., Y. O. Lee, et al. (2017). "Youth use of electronic vapor products and blunts for administering cannabis." *Addictive Behaviors* **70**: 79-82.
11. Delnevo, C. D. and M. Hrywna (2006). "The relationship of cigars, marijuana, and blunts to adolescent bidi use." *Public health reports (Washington, D.C. : 1974)* **121**(5): 603-608.
12. Steigerwald, S., P. O. Wong, et al. (2018). "Smoking, Vaping, and Use of Edibles and Other Forms of Marijuana Among U.S. Adults." *Annals of Internal Medicine* **169**(12): 890-892.
13. Wadsworth, E., S. Craft, et al. (2022). "Prevalence and use of cannabis products and routes of administration among youth and young adults in Canada and the United States: A systematic review." *Addictive Behaviors* **129**: 107258.
14. Moreno, V. M., López-López, M., Atoche, J. C., & García-Ruiz, C. (2014). Raman identification of drug of abuse particles collected with colored and transparent tapes. *Science & Justice*, *54*(2), 164-169.
15. Bumbrah, G. S. and R. M. Sharma (2016). "Raman spectroscopy – Basic principle, instrumentation and selected applications for the characterization of drugs of abuse." *Egyptian Journal of Forensic Sciences* **6**(3): 209-215.
16. Settle, F. A. (1997). Handbook of instrumental techniques for analytical chemistry. 1997. *National Science Foundation, Arlington*.
17. Lupoi, J., E. Gjersing, et al. (2015). "Evaluating Lignocellulosic Biomass, Its Derivatives, and Downstream Products with Raman Spectroscopy." *Frontiers in Bioengineering and Biotechnology* **3**.

18. Sigworth, K. (2020). Raman Spectroscopy Study of Delta-9-Tetrahydrocannabinol and Cannabidiol and their Hydrogen-Bonding Activities.
19. Number of Vibrational Modes in a Molecule. (2021, September 26). <https://chem.libretexts.org/@go/page/1857>
20. Polarizability. (2022, February 27). <https://chem.libretexts.org/@go/page/1663>
21. Ramachandran, K. I., Deepa, G., & Namboori, K. (2008). *Computational chemistry and molecular modeling: principles and applications*. Springer Science & Business Media.
22. Morin, D., *Introduction to Classical Mechanics*. Cambridge University Press: 2005.
23. Verville, G. (2020). Raman Spectroscopic and Quantum Chemical Investigation of the Effects of Tri-Methylamine N-Oxide (TMAO) On Hydrated Urea, Hydrated Guanidinium, and Hydrogen Bonded Networks.
24. Neese, F.; Bredow, T.; Wennmohs, F., *Introduction to Computational Chemistry: Fundamentals and Goals of Computational Chemistry*. Universität Bonn: 2007.
25. Hod, O., *Molecules: The Born-Oppenheimer Approximation*. Tel-Aviv University: 2010.
26. Iyengar, S. S., *The Born-Oppenheimer approximation, the Many Electron Hamiltonian and the molecular Schrodinger Equation*. Indiana University C561, Atomic and Molecular Quantum Theory 2020.
27. Feiguin, A. E., *The Born-Oppenheimer approximation*. Northeastern University Northeastern University Department of Physics 2009.

28. Nadykto, A. B., A. Al Natsheh, et al. (2008). Chapter 21 - Computational Quantum Chemistry: A New Approach to Atmospheric Nucleation. Advances in Quantum Chemistry. M. E. Goodsite and M. S. Johnson, Academic Press. **55**: 449-478.
29. Zhao, Y.; Truhlar, D. G., Density Functional for Spectroscopy: No LongRange Self-Interaction Error, Good Performance for Rydberg and ChargeTransfer States, and Better Performance on Average than B3LYP for Ground States. *Journal of Physical Chemistry A* 2006, 110 (49), 13126–13130.
30. Sherrill, D. C., Basis Sets in Quantum Chemistry. Georgia Institute of Technology: Chem 6485: Computational Chemistry, 2008.
31. Sherrill, D. C., Chem 6485, Background: Basis Sets. Georgia Institute of Technology: Sherrill Research Group Website 2009.
32. *A New Basis Set Exchange: An Open, Up-to-date Resource for the Molecular Sciences Community*. Benjamin P. Pritchard, Doaa Altarawy, Brett Didier, Tara D. Gibson, Theresa L. Windus. *J. Chem. Inf. Model.* **2019**, 59(11), 4814-4820.
33. Frisch, M. J., G. W. Trucks, et al. (2016). Gaussian 16 Rev. C.01. Wallingford, CT.
34. Sure, R., J. G. Brandenburg, et al. (2016). "Small Atomic Orbital Basis Set First-Principles Quantum Chemical Methods for Large Molecular and Periodic Systems: A Critical Analysis of Error Sources." ChemistryOpen **5**(2): 94-109.
35. Wiberg, K. B. (2004). "Basis set effects on calculated geometries: 6-311++G** vs. aug-cc-pVDZ." Journal of Computational Chemistry **25**(11): 1342-1346.
36. Kupka, T., M. Stachów, et al. (2011). "From CCSD(T)/aug-cc-pVTZ-J to CCSD(T) complete basis set limit isotropic nuclear magnetic shieldings via affordable DFT/CBS calculations." Magnetic Resonance in Chemistry **49**(5): 231-236.